IMMUNOLOGY

Single–amino acid variants in target epitopes can confer resistance to antibody-based therapies

Romina Marone[1,2]†, Erblin Asllanaj[3,4]†, Giuseppina Capoferri[1,2], Torsten Schwede[3,4], Lukas T. Jeker[1,2,5]*‡, Rosalba Lepore[1,2]*‡

Monoclonal antibodies have transformed the therapeutic landscape across oncology, immunology, and infectious diseases by enabling high-affinity, antigen-specific targeting to neutralize soluble molecules, block cellular interactions, or deplete cells. Although high specificity is critical for safety, it may confer an inherent susceptibility to even minor variations in the target epitope. Here, we investigated the impact of natural single-nucleotide variants on antigen recognition by therapeutic monoclonal antibodies, both approved and in clinical development. For almost every antibody analyzed, we identified protein variants in or near the antibody-antigen interface, a subset of which were predicted to disrupt antigen recognition. Experimental studies corroborated the impact of select variants for four different antigens, revealing complete loss of antibody binding in some cases. For example, a human breast cancer cell line overexpressing human epidermal growth factor receptor 2 (HER-2), but engineered to carry the HER-2^{P594H} variant, was completely resistant to killing even by highly potent clinical antibody-drug conjugates. These findings suggest that natural variants can confer primary resistance to antibody-based therapies, with critical implications for treatment outcomes, patient management, and safety, particularly in the context of potent modalities such as antibody-drug conjugates. Individual resistance-associated variants, although globally rare, are enriched in specific populations, underscoring the importance of accounting for genetic diversity in both drug development and clinical decision-making.

INTRODUCTION

The success of monoclonal antibodies (mAbs) for medical applications is rooted in their extraordinary diversity, affinity, and specificity, enabling targeting across a broad range of antigens and making them powerful diagnostic and therapeutic tools (*1*). Antibodies recognize and bind their target antigens through complementarity-determining regions (CDRs), interacting with specific sites of the antigens known as epitopes. A few amino acid residues in a given epitope are critical for the mAb-antigen (mAb-Ag) interaction. Some antibodies can even discriminate differences as small as a single–amino acid substitution (*2*, *3*), and picomolar binding affinities can be reached. These properties enabled modern antibody development and engineering, fueling a major industry (*1*, *4*, *5*). In 1986, the first commercial mAb was approved for T cell depletion (*4*), and, later, a CD20-directed B cell–depleting mAb became the standard of care to treat B cell lymphomas (*6*). Today, more than 100 antibody-based therapeutics are approved for many different diseases (*1*). Thus, the development of diagnostic and therapeutic mAbs revolutionized biology and medicine (*1*, *4*, *5*, *7*).

Therapeutic antibodies can exert their function through immune-mediated mechanisms such as antibody-dependent cellular cytotoxicity (ADCC), antibody-dependent cellular phagocytosis (ADCP), and complement-dependent cytotoxicity (CDC) or by delivering cytotoxic payloads as antibody-drug conjugates (ADCs). Fc engineering can silence unwanted effector activity when pure blockade is desired. Examples of therapeutic antibodies using these modes of action include rituximab (CD20, ADCC), trastuzumab emtansine and trastuzumab deruxtecan [human epidermal growth factor receptor 2 (HER-2, ADC)], and nivolumab and pembrolizumab [programmed cell death protein 1 (PD-1), blockade] (*6*, *8*–*10*). Antibodies can also be engineered as bispecific T cell engagers (*5*, *11*, *12*), or as single-chain variable fragments, used in chimeric antigen receptors (CARs) (*13*). Multiple CAR products are currently commercially available, with more than 30,000 patients treated and rapidly growing in use (*14*). Many other advanced antibody-based therapeutic formats are being developed, as recently reviewed (*1*, *5*). Collectively, antibody-derived therapies benefit millions of patients annually and constitute a major economic sector (*5*).

A common challenge in selecting a target antigen for a new antibody-based therapy is that antigens are often not restricted to the specific cell of interest but are also expressed by essential cells that should not be targeted. To overcome this challenge, we and others recently developed a concept emerging as "epitope engineering," which is based on the observation that mAbs can discriminate epitopes that differ by a single amino acid (*3*). Briefly, therapeutic cells are engineered to become resistant to an antigen-specific therapy (*15*–*19*). We have demonstrated that substituting the key residues in an epitope using genome engineering can abolish mAb binding to the engineered cells (*17*). Specifically, designed single–amino acid substitutions are sufficient to completely abolish binding and consequently cytotoxicity mediated by ADCC, T cell engagers, and even highly potent ADCs or CAR T cells (*15*, *16*, *18*, *19*). Epitope engineering was successfully applied to human CD45, CD117, CD123, and CD135, respectively (*15*, *16*, *18*–*20*). Therefore, rendering therapeutic cells resistant to antibody-derived therapy can be used to create selectivity for diseased (nonengineered) cells. We used flow cytometry to demonstrate that the epitope engineering only affects the binding of the therapeutic antibody of interest, whereas staining

[1]Department of Biomedicine, University Hospital Basel and University of Basel, Hebelstrasse 20, CH-4031 Basel, Switzerland. [2]Transplantation Immunology & Nephrology, University Hospital Basel, Petersgraben 4, CH-4031 Basel, Switzerland. [3]Biozentrum, University of Basel, Spitalstrasse 41, CH-4056 Basel, Switzerland. [4]SIB Swiss Institute of Bioinformatics, Spitalstrasse 41, CH-4056 Basel, Switzerland. [5]Innovation Focus Cell Therapies, University Hospital Basel, Petersgraben 4, CH-4031 Basel, Switzerland.
†These authors contributed equally to this work.
*Corresponding author. Email: lukas.jeker@unibas.ch (L.T.J.); rosalba.lepore@unibas.ch (R.L.)
‡These authors contributed equally to this work.

with a second, nontherapeutic "control" antibody that binds a different epitope remained unchanged (*16*–*18*, *20*). We noted that single–amino acid substitutions that achieved complete shielding included naturally occurring variants. For instance, the E51K variant of CD123 (the interleukin-3 receptor subunit α), which results from a naturally occurring single-nucleotide variant (SNV) in the *IL3RA* gene, completely abolished binding of the high-affinity mAb CSL362 (*18*). On the basis of these findings and considering the rapid expansion of antibody-based therapies in terms of both therapeutic formats and patient populations (*5*), we hypothesized that, collectively, human genetic variation could affect the clinical efficacy of antigen-specific immunotherapies, although individual variants may be rare. A literature search confirmed that a single missense mutation in the gene encoding the complement protein C5 resulted in a poor response to treatment with eculizumab (*21*). Here, we systematically analyzed the prevalence of naturally occurring SNVs across human therapeutic antigens and examined how the resulting protein variants may affect the binding of therapeutic antibodies, both approved and in clinical development.

RESULTS

Natural missense variants occur in regions coding for mAb epitopes

The dataset analyzed in this study includes 87 distinct mAb sequences encompassing a wide range of clinical stages, molecular targets, and therapeutic areas (Fig. 1A and data file S1). Among these, 44 mAbs are approved for clinical use, whereas the remaining are in various phases of clinical development (phases 1 to 3). The therapeutic areas represented include oncology (40 mAbs), immunology (28 mAbs), hematology (8 mAbs), neurology (7 mAbs), and other indications (4 mAbs), such as infectious disease, pain management, musculoskeletal disorders, and eye disorders. The antibodies target 62 distinct antigens, including key targets such as PD-1 and its ligand (PD-L1), the B lymphocyte antigen CD20, the receptor tyrosine-protein kinase HER-2, and others, with some being targeted by multiple mAbs. This diverse dataset offers a comprehensive snapshot of the current landscape of therapeutic antibody development (*22*, *23*).

For each antibody, we analyzed available three-dimensional (3D) structures of mAb-Ag complexes to define the epitope as the set of amino acid residues at the interface of the complex. We subsequently assessed the occurrence of genetic missense variants affecting epitope residues using a comprehensive dataset derived from population-wide studies. Among 25,453 distinct variants associated with the therapeutic targets in our dataset, 10,352 mapped to structurally determined protein regions, of which 1389 corresponded to epitope regions. For every antibody in our dataset, we identified multiple missense variants in their epitope regions, with the only exception being the transforming growth factor–β1 (TGF-β1) epitope recognized by fresolimumab. All other analyzed epitopes, including those formed by fresolimumab with its alternative targets (TGF-β2 and TGF-β3), contained multiple SNV sites (Fig. 1B). On average, ~50% of the residues in epitope regions were annotated with one or more missense variants on the basis of our dataset.

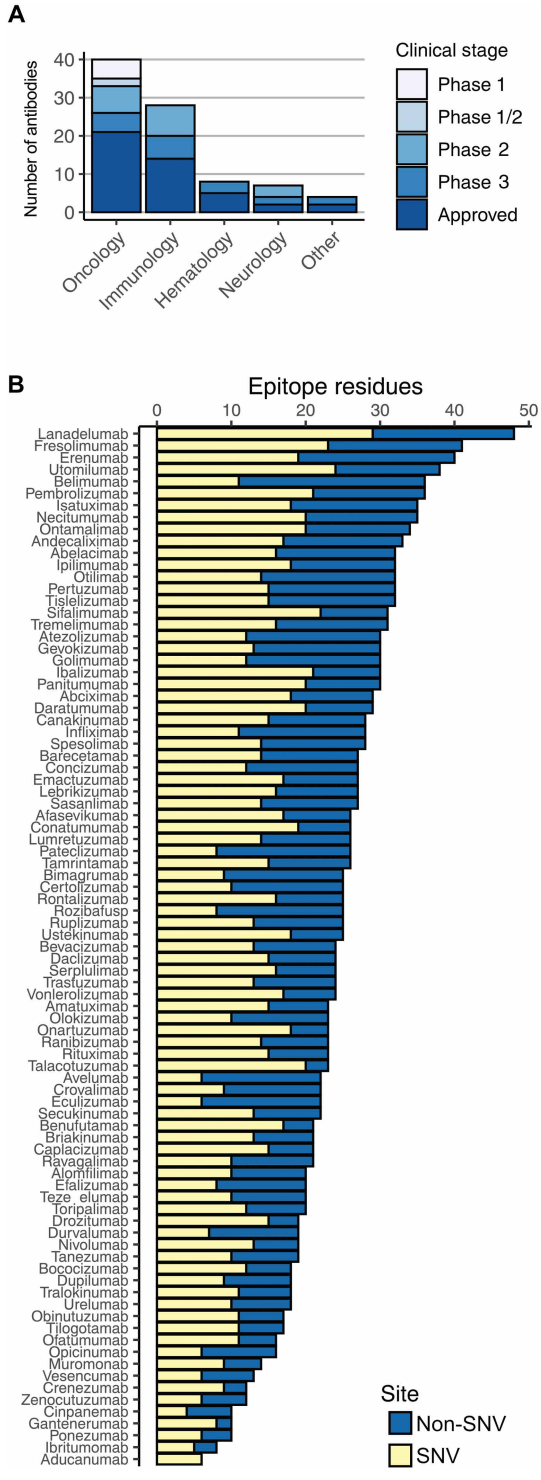

Fig. 1. Naturally occurring missense variants are observed across mAb epitopes. (**A**) Distribution of antibodies by clinical stage and therapeutic indications. (**B**) Distribution of SNV sites across antibody epitopes. Numbers of antigen-binding residues are colored by the presence (yellow) or absence (blue) of SNVs in this dataset.

Missense variants are predicted to alter antibody binding and antigen stability

To estimate the effect of SNV-associated amino acid variants, we used a structure-based computational approach relying on an empirical force field to calculate the free energy change ($\Delta\Delta G$) between the wild-type (WT) and the SNV mutant amino acid (*24*). We predicted the $\Delta\Delta G$ for each variant, comparing their effect on the stability of the mAb-Ag complex versus the antigen alone; we also predicted

the mutational impact by AlphaMissense (AM) (*25*) (Fig. 2A). Variants with $\Delta\Delta G > 1$ (mAb-Ag complex) were predicted to affect antibody binding to the antigen, whereas variants with $\Delta\Delta G > 1$ (antigen) were predicted to disrupt antigen stability, which could indirectly affect antibody binding as well (*26*). Approximately 50% of the variants were predicted to be neutral, i.e., showing a $\Delta\Delta G \leq 1$ for both the antibody-antigen complex and the antigen. The remaining were predicted to affect stability, with ~20% affecting antibody binding while being tolerated by the antigen and ~30% affecting antigen stability and antibody binding. Variants predicted to affect antigen stability tended to show higher average AM scores with a substantial proportion predicted as "ambiguous" or "likely pathogenic" by AM (Fig. 2A and fig. S1A). To classify variants based on their predicted effect, we computed the consensus between both predictions (Fig. 2B) and plotted the resulting SNV classification for each antibody (Fig. 2C). Specifically, 41% of variants were predicted to be neutral by both methods, 10% were predicted to affect the antigen itself, and 15% were predicted to interfere with antibody binding. The variants predicted to interfere with antibody binding were those predicted to affect the stability of the mAb-Ag complex but have a neutral effect on the antigen according to both methods. The remaining 34% of variants were classified as uncertain, encompassing variants where the two prediction methods yielded conflicting results (e.g., $\Delta\Delta G < 1$ and likely pathogenic by AM), as well as variants for which AM predicted an ambiguous effect (fig. S1B), representing approximately one-third of the uncertain category. As expected, epitope residues associated with SNVs predicted to affect antigen structure or function were typically more buried and exhibited low sequence variability in multiple sequence alignments (MSAs) (fig. S1, C and D). Conversely, residues associated with

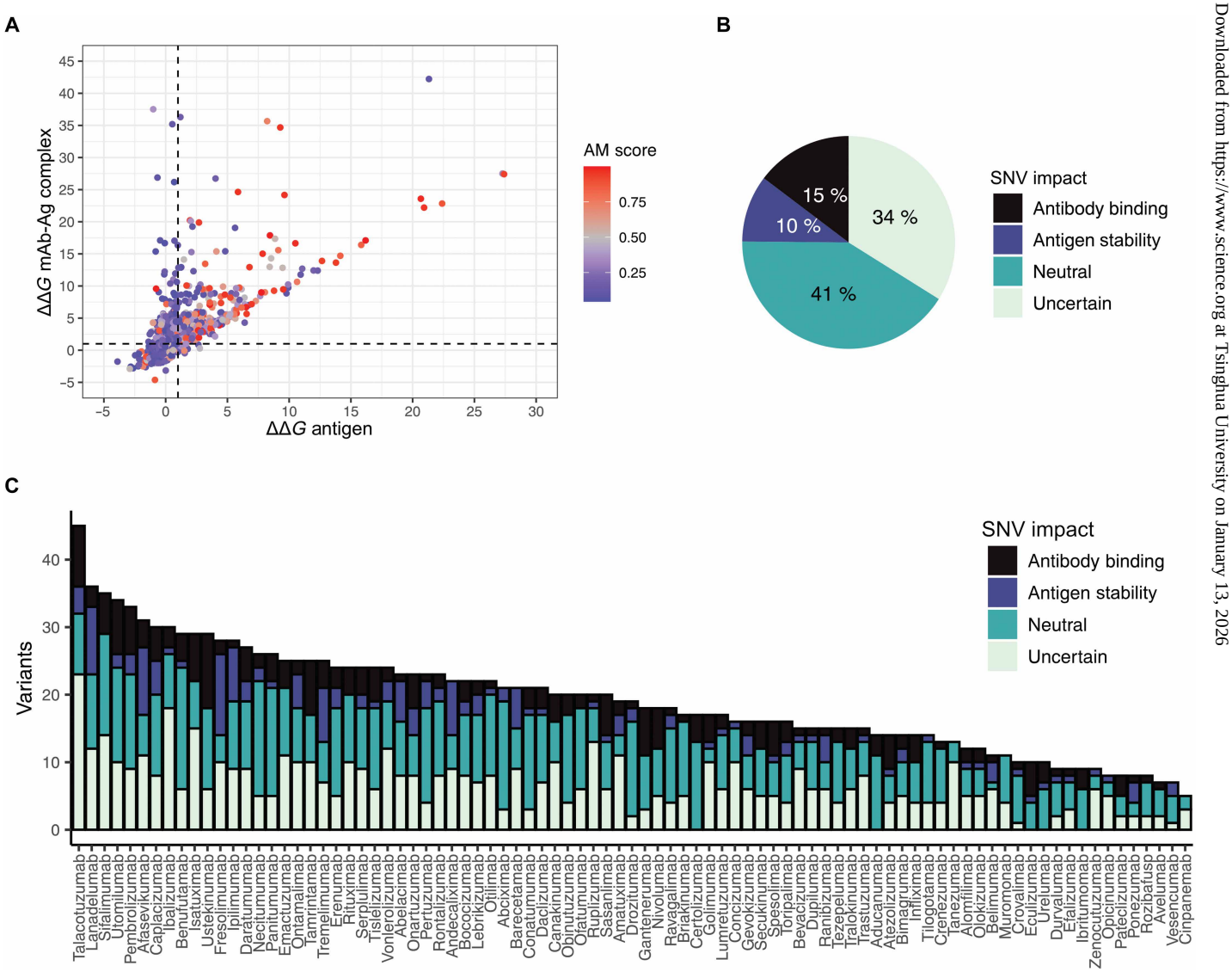

Fig. 2. Missense variants are predicted to alter antibody binding and antigen stability. (**A**) Predicted $\Delta\Delta G$ for missense epitope variants on mAb-Ag complexes (*y* axis) versus antigens alone (*x* axis). Data points are color coded on the basis of AM scores. Variants with low AM scores (predicted "likely benign" by AM) are shown in blue, high scores (predicted likely pathogenic by AM) are shown in red, and intermediate scores (predicted ambiguous by AM) are shown in gray. (**B** and **C**) Classification of SNV impact based on consensus (or lack thereof) between structure-based predictions and AM scores across the full dataset (B) and by individual epitopes (C).

SNVs predicted to be neutral for the antigen or only affecting antibody binding displayed high solvent accessibility and sequence variability. Furthermore, SNVs predicted to affect antigen structure or function contained a notable proportion of known disease-associated variants (fig. S1E). In summary, 84 of the 87 antibodies in our dataset bound to epitopes for which we identified multiple SNVs predicted to either affect antibody binding or to affect the antigen itself (Fig. 2C). Among these, we accurately predicted the effects of variants known to abolish antibody binding, such as $C5^{R885H}$, which was shown to cause therapy failure with eculizumab (*21*), and $CD38^{S274F}$, which was shown to disrupt daratumumab binding (*27*). Furthermore, we correctly predicted the effects of multiple CD123 variants, including E51K, which we previously showed to abolish talacotuzumab binding, and S59P, which affects both talacotuzumab and interleukin-3 binding (data file S2) (*18*).

To investigate these results further, we selected CD20 (rituximab), CD38 (daratumumab and isatuximab), PD-1 (nivolumab and pembrolizumab), and HER-2 (trastuzumab and pertuzumab) for a more in-depth characterization and experimental validation. This selection was guided by computational predictions to include predicted neutral or impactful variants, clinical relevance, SNV frequency, antibody availability, and mode of action (data file S3).

SNVs in the gene encoding CD20, *MS4A1*, affected binding of B cell–depleting antibodies

CD20 is a key drug target for B cell depletion therapy in B cell lymphomas and autoimmune diseases (*28*, *29*). The introduction of CD20-targeting mAbs such as rituximab, a very successful mAb that rapidly became the standard of care to treat B cell lymphomas (*6*), has driven the development of successive generations of anti-CD20 antibodies, including ofatumumab. The epitopes of rituximab and ofatumumab are distributed across two extracellular loops (ECL1, residues 70 to 82; ECL2, residues 142 to 182). According to our analysis, the *MS4A1* genomic region coding for these loops hosts multiple SNV sites (Fig. 3A). Rituximab binds to the dimeric form of CD20 in a 2:2 stoichiometry (Fig. 3B), with an interaction interface primarily mediated by ECL2 and the rituximab heavy-chain CDRs (Fig. 3, B and C) (*30*). Ofatumumab, a second-generation mAb, also binds CD20 in a 2:2 stoichiometry but with a distinct geometry (Fig. 3D), with the ECL2 interacting with both the heavy- and light-chain CDRs (Fig. 3, D and E), previously shown to result in more efficient complement recruitment (*31*, *32*). Most identified variants are predicted to have a neutral effect on mAb binding, as well as on the structure and function of the protein (Fig. 3A), with some exceptions. Among these, variant N171Y shows the highest allele frequency according to gnomADv4.1 (data file S3). Residue N171 is in the C-terminal region of the ECL2 loop, in the ^{170}ANPS^{173} motif, and is a critical recognition site for several anti-CD20 antibodies, including rituximab (*33*–*35*). Computational predictions suggested a differential impact of the N171Y variant on rituximab and ofatumumab binding (Fig. 3A). Analysis of the experimental structure of the mAb-Ag complex revealed that N171 directly interacts with rituximab's heavy-chain loop H3 (residue range, S95 to V102) through a hydrogen bond with S95 and van der Waals interactions with W100B (H3) and H35 (Fig. 3C). In contrast, in the CD20-ofatumumab interface, N171 primarily interacts with residue W94 of the light-chain loop L3 (residue range, Q89 to T97) through a polar-π interaction. A key interaction involves the adjacent residue CD20 E174, which forms a hydrogen bond with S56 on the heavy-chain loop H2 (residue range, S52 to S56) of ofatumumab (Fig. 3E). This distinct interaction pattern might explain the predicted resilience of ofatumumab to the N171Y variant.

To validate the computational predictions, we expressed $CD20^{WT}$ and eight CD20 variants for residues 168, 170, 171, 174, and 178 that reflect different predicted impact. We expressed the proteins in chicken DF-1 cells because they do not naturally express human CD20 and therefore provide a very good signal-to-noise ratio for analyzing antibody binding by flow cytometry. In addition to the therapeutic antibody of interest, rituximab, we used two research use–only control antibodies (clones S18015E and 2H7) of which the chimeric 2H7 mAb binds to the ^{170}ANPS^{173} motif in the C-terminal region of the ECL2 loop (*33*). We previously found that flow cytometry staining using a pair of mAbs represents a sensitive assay to determine the effect of SNVs affecting mAb binding to extracellular domains (*16*, *18*). $CD20^{WT}$-expressing cells were double stained with the clinical rituximab biosimilar product (Rixathon) and each of the control antibodies. However, $CD20^{N171Y}$-expressing cells were not bound by Rixathon or either control antibody, suggesting that $CD20^{N171Y}$ affected binding of all three antibodies (Fig. 3F and fig. S2). In contrast, staining with an ofatumumab research biosimilar was preserved, confirming the expression of the N171Y variant, whereas binding of the control mAbs was again abolished (Fig. 3G and fig. S2). Thus, in line with our computational analysis, $CD20^{N171Y}$ specifically abolishes the binding of Rixathon but not the ofatumumab research biosimilar (fig. S2). Other CD20 variants affected antibody binding to different degrees. For instance, $CD20^{E174A}$ and $CD20^{E174K}$ showed a near complete loss of binding to Rixathon but not to the ofatumumab research biosimilar (fig. S2), whereas $CD20^{A170P}$, $CD20^{A170S}$, and $CD20^{A170T}$ had an intermediate impact on Rixathon binding (fig. S2). Some of these results diverged from predictions, supporting the value of combining computational methods, structural inspection, and experimental validation.

SNVs in *CD38* affected daratumumab and isatuximab binding

Daratumumab and isatuximab are the two anti-CD38 mAbs currently approved for the treatment of multiple myeloma. Their interaction with CD38 triggers various downstream mechanisms, including ADCC, ADCP, and CDC (*36*), leading to effective antitumor activity. These mAbs target distinct CD38 epitopes (Fig. 4, A and B). Isatuximab binds to the catalytic region of CD38, exhibiting strong proapoptotic activity independent of cross-linking agents, unlike daratumumab (*37*, *38*). Epitope regions of both antibodies were associated with multiple SNV sites (Fig. 4A). Among these, the $CD38^{G113R}$ variant was predicted to have the strongest impact on isatuximab binding, with potential consequences on the antigen itself (Fig. 4, A and C). In addition, $CD38^{G113E}$, $CD38^{T148K}$, $CD38^{T148M}$, $CD38^{T148R}$, and $CD38^{R194H}$ were predicted to affect isatuximab binding. Predictions at position K111 indicated a neutral effect for the conservative $CD38^{K111R}$ variant and an impactful effect for $CD38^{K111N}$. For daratumumab, the $CD38^{S274F}$ variant was predicted to substantially impair antibody binding, in agreement with previous findings (*27*). In contrast, variants at residue W241, which is central to a β sheet, were predicted to affect the antigen itself (Fig. 4, A and D), potentially causing local perturbations that might alter the binding of the antibody. $CD38^{W241S}$ was predicted to possibly show a pronounced effect.

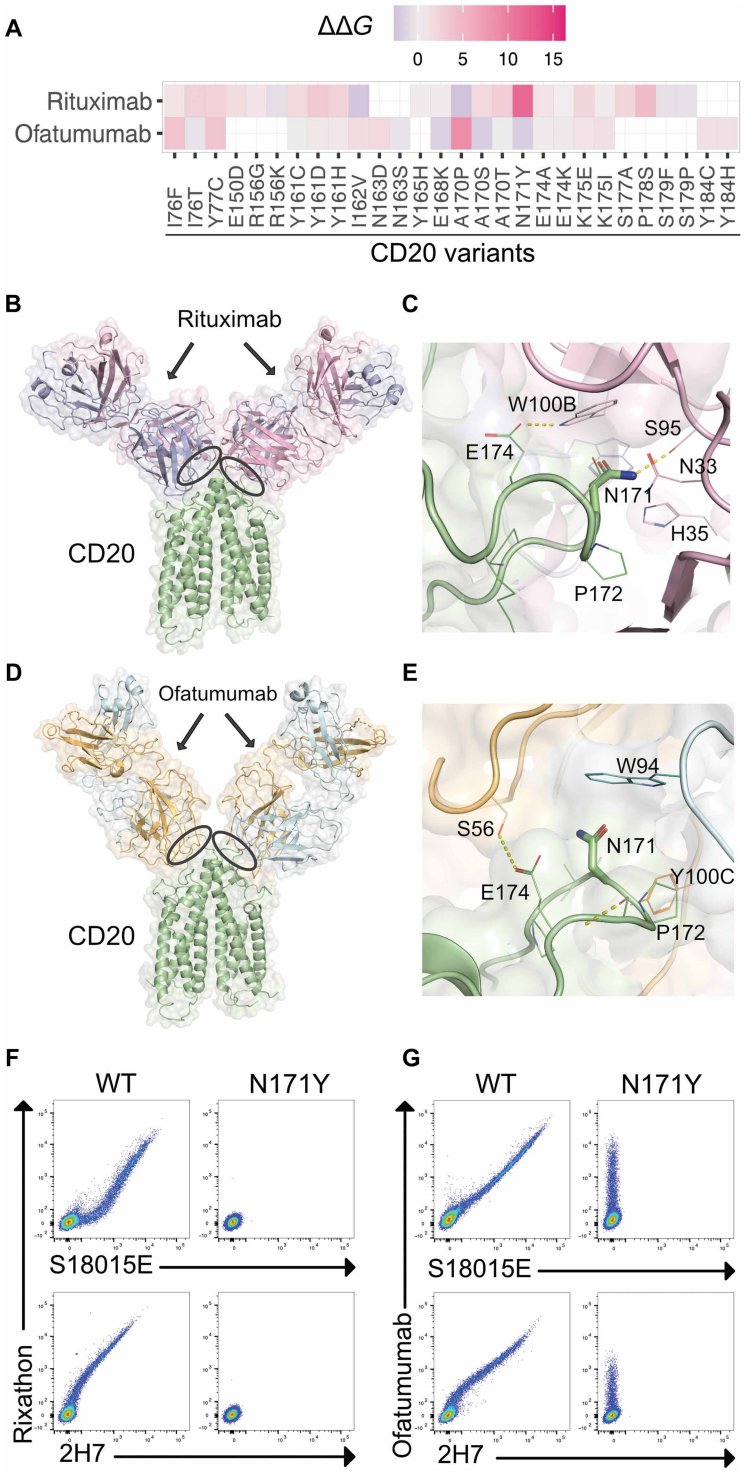

Fig. 3. The CD20 N171Y variant abolishes the binding of rituximab but not ofatumumab antibodies. (**A**) Predicted ΔΔ*G* for missense epitope variants in the CD20-rituximab and CD20-ofatumumab complexes, represented as a heatmap. (**B**) 3D structure of the 2:2 CD20-rituximab complex (PDB ID: 6Y90). The CD20 antigen is shown in green, with the rituximab heavy chain in pink and light chain in blue. (**C**) Close-up view of the N171 residue at the CD20-rituximab interface. Residue N171 is depicted as a stick, with neighboring CD20 residues (green) and rituximab residues (pink and blue) shown as lines. (**D**) 3D structure of the 2:2 CD20-ofatumumab complex (PDB ID: 6Y92). The CD20 antigen is shown in green, with the ofatumumab heavy chain in light blue and light chain in orange. In (B) and (D), ovals indicate the locations of SNV sites at the interface of the complex. (**E**) Close-up view of the N171 residue at the CD20-ofatumumab interface. Residue N171 is depicted as a stick, with neighboring CD20 residues (green) and ofatumumab residues (light blue and orange) shown as lines. In (D) and (E), antibody residues are labeled according to the Chothia numbering scheme, and hydrogen bonds are indicated with yellow dashed lines. (**F** and **G**) Flow cytometry histograms show staining of WT CD20 or the N171Y variant overexpressed in DF-1 cells. Various combinations of staining using the mAbs Rixathon, S18015E, and 2H7 (F) or ofatumumab research biosimilar, S18015E, and 2H7 (G) are shown. For (F), $n = 4$ independent experiments for each group were performed. For (G), $n = 2$ independent experiments for each group were performed.

As with CD20, we validated mAb binding to $CD38^{WT}$ and CD38 carrying different SNVs using daratumumab and isatuximab research biosimilars, hereafter referred to as "daratumumab" or "isatuximab," respectively. We used clone HB-7 as a control antibody. $CD38^{WT}$-expressing cells were double stained with either daratumumab and control or isatuximab and control, respectively (Fig. 4E and fig. S3). Variants $CD38^{W241R}$, $CD38^{W241S}$, and $CD38^{S274F}$ selectively affected daratumumab staining but not control antibody nor isatuximab staining (Fig. 4E and fig. S3), consistent with predictions. $CD38^{W241R}$ and $CD38^{S274F}$ completely abolished daratumumab staining, whereas $CD38^{W241S}$ reduced staining almost completely. Thus, $CD38^{W241R}$, $CD38^{W241S}$, and $CD38^{S274F}$ will likely result in resistance to daratumumab treatment. In contrast, $CD38^{G113E}$ and $CD38^{G113R}$ partially affected isatuximab staining but did not affect daratumumab binding (Fig. 4E, fig. S3, and data file S3). Similarly, in line with predictions, we observed impaired isatuximab staining for $CD38^{K111N}$ but not for $CD38^{K111R}$ and impaired isatuximab staining for variants $CD38^{T148M}$, $CD38^{T148K}$, and $CD38^{T148R}$ (Fig. 4E and fig. S3). These data suggest that isatuximab treatment may be less effective in patients carrying these variants, with varying degrees of resistance for $CD38^{K111N}$, $CD38^{G113E}$, $CD38^{G113R}$, $CD38^{T148K}$, and $CD38^{T148R}$, but remains unaffected by variants that impair daratumumab binding (e.g., $CD38^{W241R}$, $CD38^{W241S}$, and $CD38^{S274F}$).

PD-1 variants differentially impair binding of pembrolizumab and nivolumab

The therapeutic mAbs targeting the B cell lineage targets CD20 and CD38 are cell-depleting antibodies. Next, we analyzed blocking antibodies using checkpoint inhibitors. These antibodies do not directly target tumor cells but rather block an inhibitory signal provided by tumor cells that engage, e.g., PD-1 on T cells. As a result, cytotoxic T cells become dysfunctional and lose their ability to kill the cancer cells. Blocking PD-1–mediated signaling can restore T cell function, resulting in tumor elimination (*9*, *39*–*41*). We identified multiple SNVs at different PD-1 residues that might affect nivolumab or pembrolizumab binding. Among these, variants at residues S87, P89, and G90 were predicted to have strong impact on pembrolizumab binding, whereas variants at residue P28 are expected to affect nivolumab binding (Fig. 5A). S87, P89, and G90 are located on a loop that serves as a primary anchor point for pembrolizumab, positioned in a groove at the interface of the heavy- and light-chain CDR loops (Fig. 5, B and C). Conversely, P28 primarily interacts

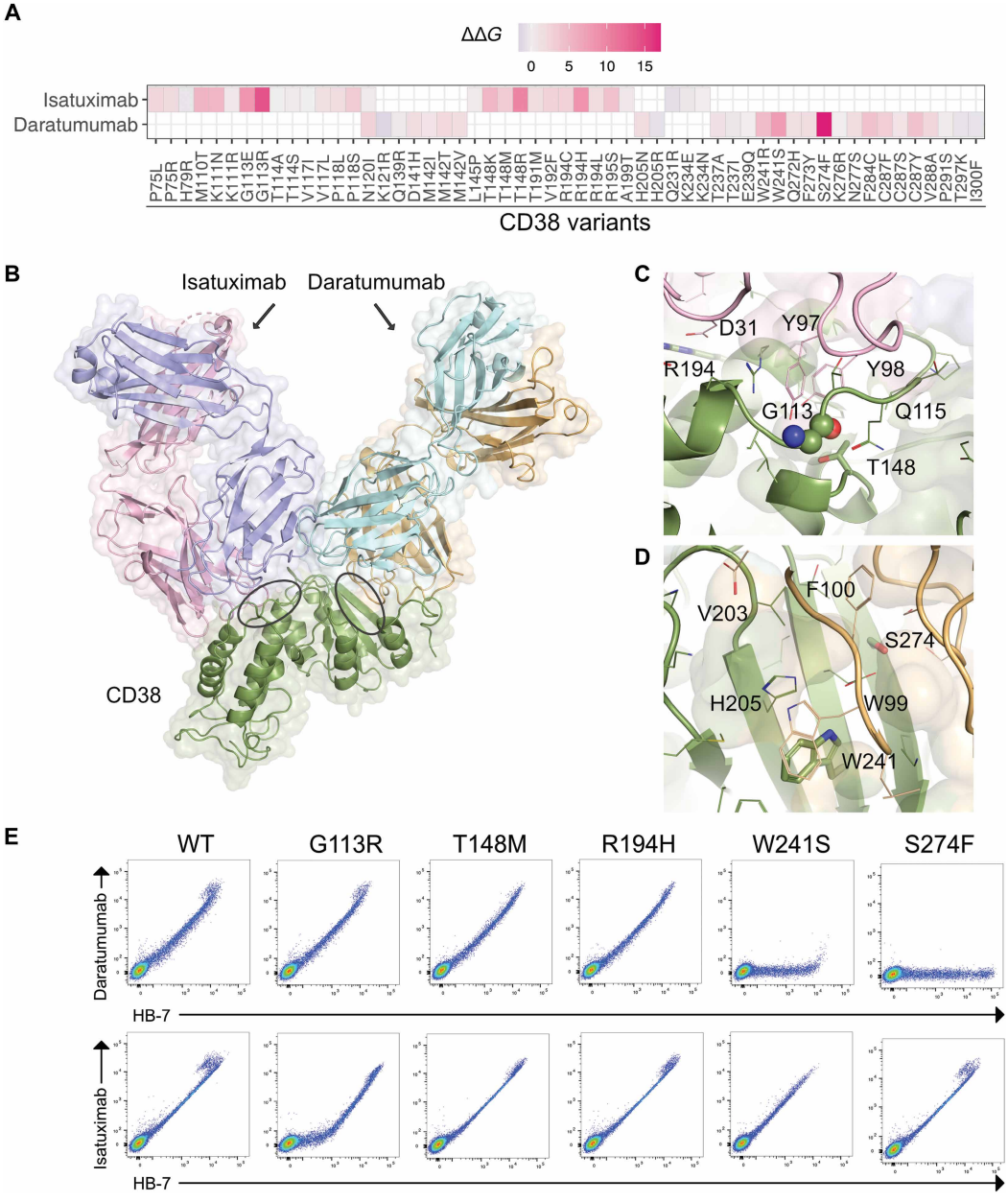

Fig. 4. Impact of CD38 epitope variants on the binding of isatuximab and daratumumab antibodies. (**A**) Predicted ΔΔ*G* for missense epitope variants in the CD38-isatuximab and CD38-daratumumab complexes, represented as a heatmap. (**B**) 3D structure representation of the CD38 extracellular domain in complex with isatuximab (PDB ID: 4CMH) and daratumumab (PDB ID: 7DHA). The visualization is derived from the structural superposition of CD38 (green). The isatuximab heavy chain is shown in pink, and its light chain is shown in blue. Daratumumab heavy chain is shown in light blue, and its light chain is shown in orange. Ovals indicate the locations of SNV sites at the interface of the complex. (**C**) Close-up view of key epitope residues (G113, T148, and R194) at the CD38-isatuximab interface. The residues are shown as sticks (G113 main chain atoms as spheres), with neighboring CD38 residues (green) and isatuximab residues (pink and blue) shown as lines. (**D**) Close-up view of key epitope residues (W241 and S274) at the CD38-daratumumab interface. The residues are shown as sticks, with neighboring CD38 residues (green) and daratumumab residues (light blue and orange) shown as lines. In (C) and (D), antibody residues are labeled according to the Chothia numbering scheme. (**E**) Flow cytometry histograms show staining of WT CD38 or variants overexpressed in DF-1 cells. Staining was performed using daratumumab or isatuximab research biosimilars combined with HB-7. For (E), $n = 1$ or 2 independent experiments for each group were performed.

with W52 of the nivolumab heavy chain (Fig. 5, D and E). Several variants at positions P28, D85, S87, P89, and G90, predicted to affect antibody binding to varying degrees, were selected for testing.

All mutants were stained for the control antibody NAT105 and nivolumab or pembrolizumab research biosimilars, hereafter referred to as "nivolumab" or "pembrolizumab," respectively (Fig. 5F and fig. S4). Contrary to predictions, neither PD-1^{P28L} nor PD-1^{P28S} affected binding of nivolumab. In contrast, PD-1^{D85N}, PD-1^{S87R}, PD-1^{P89L}, PD-1^{P89R}, and PD-1^{P89T} abolished pembrolizumab but not nivolumab binding (Fig. 5F and fig. S4). PD-1^{S87N}, PD-1^{G90S}, and PD-1^{G90V}

resulted in some loss of binding to pembrolizumab. Thus, we found five SNVs at three different residues that prevented pembrolizumab binding but none affecting nivolumab.

Genetic variation affects antibodies that bind HER-2

Last, we analyzed HER-2, a target found in epithelial tissues. About 20% of breast cancers and some ovarian and gastric cancers overexpress *ERBB2*, the gene encoding HER-2, providing the tumor cells a growth advantage (*10*). Because HER-2 overexpression is associated with a poorer prognosis, trastuzumab was generated as a first generation HER-2 targeting mAb. Trastuzumab is reported to exert its therapeutic effects through a dual mechanism, blocking ligand-independent dimerization and signaling (*42*) and mediating ADCC (*10*, *43*, *44*). Although trastuzumab combined with chemotherapy has been shown to result in a substantial clinical benefit and represents a major medical advance (*8*), second-generation trastuzumab-based drugs were developed as ADCs: trastuzumab emtansine and trastuzumab deruxtecan. Both are based on the identical mAb (trastuzumab) but differ in the linker, toxic payload, and drug-antibody ratio (*5*, *45*). Trastuzumab deruxtecan is more potent in breast cancer (*45*) and approved for breast cancer and other HER-2–expressing cancers, highlighting the importance of trastuzumab-based drugs in oncology.

Trastuzumab binds the juxtamembrane region of HER-2 (domain IV), whereas pertuzumab binds to domain II (*42*), sterically blocking ligand-dependent dimerization and signaling (*46*) (Fig. 6, A and B), previously shown to result in synergistic effects when administered together (*47*). We identified several SNVs in *ERBB2* regions coding for both epitopes (Fig. 6A), with HER-2^{P594H} having the strongest effect on trastuzumab binding (Fig. 6A). Other identified variants were predicted to have minimal or no impact on antibody binding, except for HER-2^{R288W} and HER-2^{G309E}, which were predicted to affect pertuzumab binding; in addition, HER-2^{G309E} is predicted to be pathogenic by AM (Fig. 6, A and C, and data file S2). G309 is located on a small turn that connects two β strands and primarily participates in van der Waals interactions (Fig. 6C). Conversely, P594 is surrounded by aromatic side chains, including trastuzumab H3 residues Y100A and W95, mediating both intramolecular and intermolecular stacking interactions (Fig. 6D). To validate the computational predictions for HER-2, we selected multiple variants for experimental validation, including HER-2^{R288W}, HER-2^{R292S}, HER-2^{G309E}, HER-2^{P593L}, and HER-2^{P594H} (Fig. 6, E and F, and fig. S5). We first tested the binding of trastuzumab and pertuzumab research biosimilars (hereafter referred to as "trastuzumab" or "pertuzumab," respectively) without a linker-toxin payload and used a research use–only clone, 24D2, as a control antibody. HER-2^{WT} cells bound all antibodies, whereas HER-2^{G309E} mildly affected pertuzumab, but not trastuzumab, binding (Fig. 6, E and F, and fig. S5). In contrast, HER-2^{P594H} completely abolished trastuzumab binding but did not affect pertuzumab binding (Fig. 6, E and F, and fig. S5). Several other variants, including HER-2^{R288W}, had no effect on trastuzumab or pertuzumab binding (fig. S5).

A naturally occurring SNV confers resistance to clinical ADCs

We next aimed to investigate SNV-mediated resistance to two potent and frequently used ADCs, trastuzumab emtansine and trastuzumab deruxtecan (*48*). In the flow cytometry binding assays for experimental validation of the computational predictions, we used biosimilar antibodies (clinical or research). However, for ADCs, we wanted to use original clinical products because even when the same mAb is used as a basis, ADCs carry different linkers and toxins and are produced by different conjugation methods that cannot easily be reproduced, resulting in distinct molecules with specific properties (*5*, *48*). Therefore, we tested trastuzumab emtansine and trastuzumab deruxtecan with the original products Kadcyla and Enhertu, respectively. First, we analyzed HER-2 expression on two breast cancer cell lines, MDA-MB-231 and HCC1954. HER-2 expression is low on MDA-MB-231 cells, whereas the HCC1954 cell line overexpresses HER-2 (Fig. 7A). We obtained both clinical ADCs from the hospital pharmacy and titrated Kadcyla and Enhertu on each cell line. Neither ADC killed the HER-2 low cell line MDA-MB-231 at concentrations up to 2000 pM. In contrast, HCC1954 cells were killed in a dose-dependent manner by both ADCs (Fig. 7B). To test resistance, we used CRISPR-Cas9–mediated homology-directed repair (HDR) to engineer HER-2^{P594H} into HCC1954 cells. HCC1954 electroporated with single guide RNA (gRNA)/Cas9 ribonucleoprotein (RNP) resulted in HER-2 knockout (KO), as illustrated by a loss of trastuzumab and 24D2 binding (Fig. 7C). Addition of the HDR template (HDRT) encoding HER-2^{P594H} resulted in a population of cells that stained for 24D2, but not trastuzumab, indicative of the desired editing. To validate correct engineering, we used fluorescence-activated cell sorting (FACS) to purify WT (unedited), KO [nonhomologous end joining (NHEJ)], and knockin (KI; engineered) cells. Next-generation sequencing (NGS) confirmed that the WT cells remained unedited, and KO cells displayed indels, whereas most of the purified KI cells contained the intended protospacer adjacent motif (PAM) mutation to increase editing efficiency and the CCC-to-CAC codon change resulting in HER-2^{P594H} (Fig. 7D). We then tested susceptibility of unedited WT, WT-sorted (HER-2^{WT}), KO-sorted (HER-2^{KO}), and KI-sorted (HER-2^{P594H}) HCC1954 cells to Kadcyla and Enhertu. Whereas unedited WT and HER-2^{WT} cells were killed by increasing concentrations of Kadcyla and Enhertu, the HER-2^{KO} and HER-2^{P594H} cells were resistant to ADC-mediated killing (Fig. 7E). Thus, the HER-2^{P594H} SNV, when engineered into a breast cancer cell line overexpressing HER-2, resulted in resistance against the clinically used drugs Kadcyla and Enhertu.

DISCUSSION

Here, we analyzed how human genetic diversity in epitopes bound by therapeutic mAbs might affect antigen-specific therapies. We focused on approved therapeutic antibodies and antibodies in clinical development. For every analyzed antibody, we found multiple SNVs in their respective epitope regions. A substantial portion of these SNVs was predicted to alter antibody binding, either directly by disrupting the antibody-antigen interface without affecting the antigen's structure or function or indirectly by altering the structure of the antigen itself. We experimentally validated the impact of 43 SNVs located at 26 epitope residues in four target proteins. For 19 of these SNVs, we observed a reduction or complete loss of antibody binding, consistent with the computational predictions.

Our findings have implications for various patients, physicians, health care systems, and the pharmaceutical industry. First, for patients carrying a specific SNV, treatment with a drug that cannot be effective means unnecessary procedures, exposure to unwarranted safety risks, and false hope for therapeutic benefit. Although mAbs are generally well tolerated, the occurrence of infrequent but serious

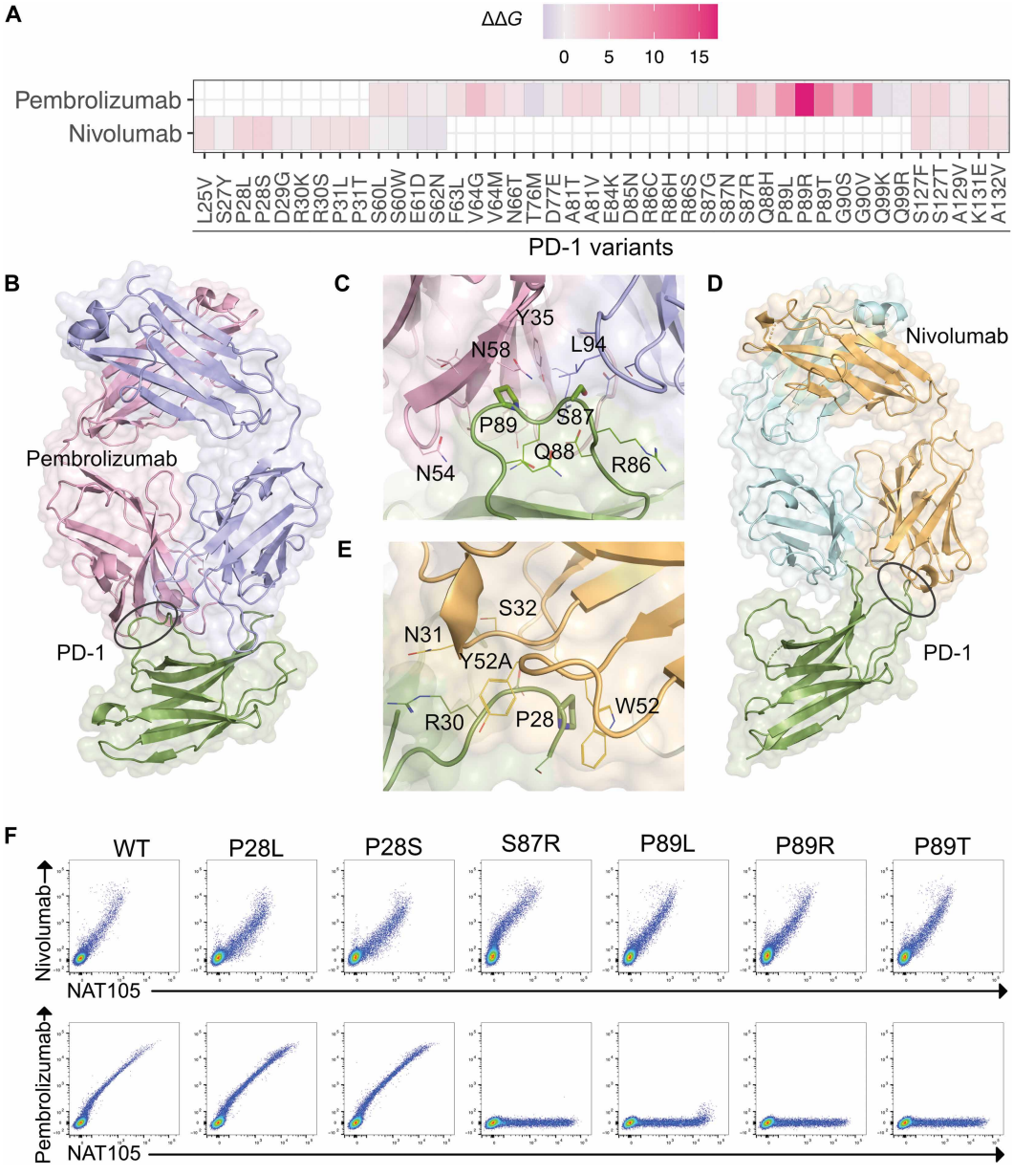

Fig. 5. Impact of PD-1 epitope variants on the binding of pembrolizumab and nivolumab antibodies. (**A**) Predicted $\Delta\Delta G$ for missense epitope variants in the PD-1–pembrolizumab and PD-1–nivolumab complexes, represented as a heatmap. (**B**) 3D structure of the PD-1–pembrolizumab complex (PDB ID: 5GGS). The PD-1 antigen is shown in green, with the pembrolizumab heavy chain in pink and light chain in blue. Ovals indicate the locations of SNV sites at the interface of the complex. (**C**) Close-up view of key epitope residues (P89 and S87) at the PD-1–pembrolizumab interface. The residues are shown as sticks with neighboring PD-1 residues (green) and pembrolizumab residues (pink and blue) shown as lines. (**D**) 3D structure of the PD-1–nivolumab complex (PDB ID: 5GGR). The PD-1 antigen is shown in green, with the nivolumab heavy chain in light blue and light chain in orange. Ovals indicate the locations of SNV sites at the interface of the complex. (**E**) Close-up view of the P28 residue at the PD-1–nivolumab interface. Residue P28 is depicted as a stick, with neighboring PD-1 residues (green) and nivolumab residues (light blue and orange) shown as lines. In (C) and (E), antibody residues are labeled according to the Chothia numbering scheme. (**F**) Flow cytometry histograms show staining of WT PD-1 or variants overexpressed in DF-1 cells. Staining was performed using pembrolizumab or nivolumab research biosimilars combined with NAT105. For (F), $n = 2$ or 3 independent experiments for each group were performed.

adverse events constitutes a concern. ADCs, on the other hand, are associated with treatment-related adverse events in ~90% of patients, with serious events (grade ≥ 3) reported in 46% of cases on average (*5*, *49*). Therefore, polymorphisms that could affect ADCs are particularly important. Frequently, ADC-related adverse events arise from target-independent effects associated with the intrinsic toxicity of the payload (*50*, *51*), a key determinant of the maximum tolerated dose (*52*). Consequently, if the ADC fails to bind to its intended target because of a resistance-causing SNV, then the entire dose is subject to potential target-independent, systemic toxicity, a highly undesirable outcome that should be avoided. Support for this comes from a terminated clinical trial (NCT04849910) investigating patients with engineered ADC resistance (through the transplantation of CD33-deficient hematopoietic stem cells) and treated with a

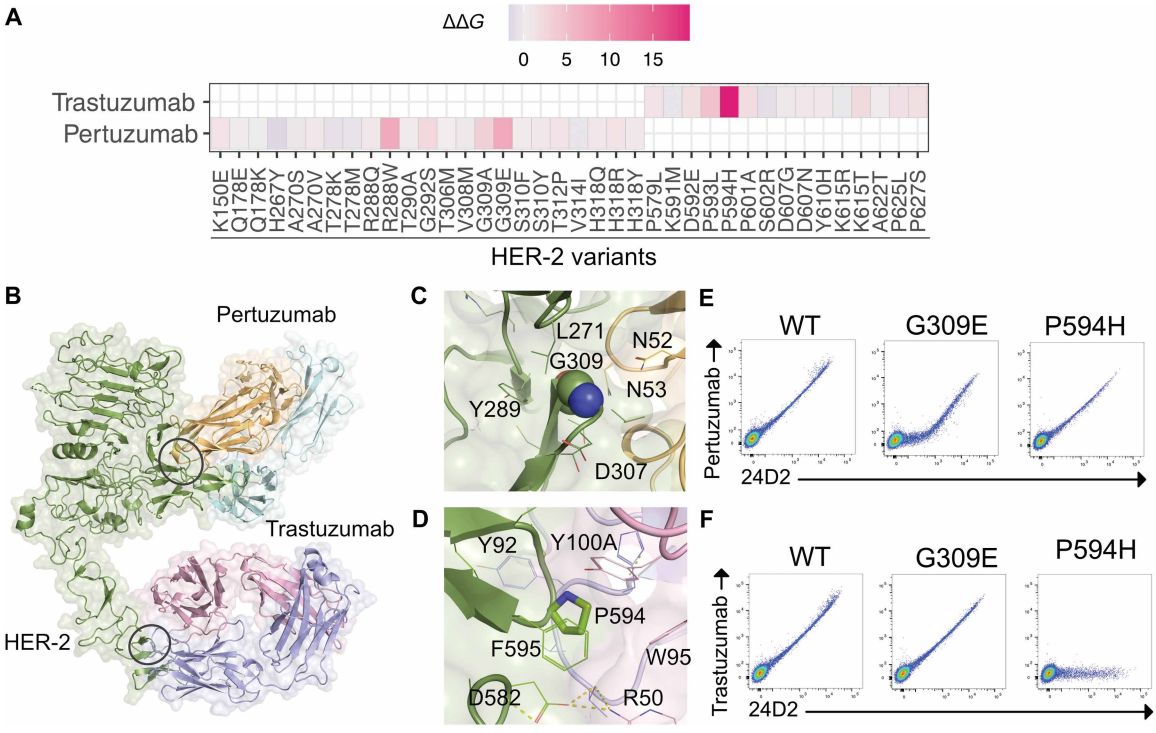

Fig. 6. Impact of HER-2 epitope variants on the binding of trastuzumab and pertuzumab antibodies. (**A**) Predicted ΔΔ*G* for missense epitope variants in the HER-2–trastuzumab and HER-2–pertuzumab complexes, represented as a heatmap. (**B**) 3D structure representation of the HER-2 extracellular domain in complex with pertuzumab (PDB ID: 1S78) and trastuzumab (PDB ID: 1N8Z). The visualization is derived from the structural superposition of HER-2 (green). The pertuzumab heavy chain is shown in light blue, and its light chain is shown in orange. Trastuzumab heavy chain is shown in pink, and its light chain is shown in blue. Ovals indicate the locations of SNV sites at the interface of the complex. (**C**) Close-up view of residue G309 at the HER-2–pertuzumab interface. Residue G309 main chain atoms are depicted as spheres, with neighboring HER-2 residues (green) and pertuzumab residues (light chain in orange) shown as lines. (**D**) Close-up view of residues P594 at the HER-2–trastuzumab interface. Residue P594 is depicted as a stick, with neighboring HER-2 residues (green) and trastuzumab residues (pink and blue) shown as lines. In (C) and (D), antibody residues are labeled according to the Chothia numbering scheme. (**E**) Flow cytometry histograms show staining of WT HER-2 or variants overexpressed in DF-1 cells. Staining was performed using pertuzumab combined with 24D2. (**F**) Flow cytometry histograms show staining of WT HER-2 or variants overexpressed in DF-1 cells. Staining was performed using trastuzumab combined with 24D2. For (E) and (F), $n = 2$ independent experiments for each group were performed.

CD33-directed ADC [gemtuzumab ozogamicin (GO)]. Compared with historic controls, low-dose GO injections resulted in higher-than-expected ADC serum concentrations, comparable to healthy individuals carrying CD33-sufficient cells that received higher GO doses. By inference, applying the recommended GO dose, which was determined in a population of CD33-sufficient patients, would likely lead to higher GO serum concentrations and an increased risk for payload-related toxicity.

Physicians must be aware of the potential for resistance due to polymorphisms in the targeted epitopes. A diagnostic test for known epitope-associated variants could help avoid ineffective treatments in patients carrying those variants and guide treatment decisions, especially when multiple antibodies are available. For instance, $CD20^{N171Y}$ results in resistance to rituximab but not ofatumumab. Therefore, for $CD20^{N171Y}$ carriers, ofatumumab should be chosen. Similarly, $CD38^{W241R}$, $CD38^{W241S}$, and $CD38^{S274F}$ result in resistance to daratumumab but not isatuximab (*27*). Therefore, a diagnostic test showing either of these variants would guide a physician to apply isatuximab rather than daratumumab. Vice versa, a patient carrying $CD38^{K111N}$, $CD38^{G113E}$, $CD38^{G113R}$, $CD38^{T148K}$, or $CD38^{T148R}$ should be treated with daratumumab rather than isatuximab. The same applies to other targets; for example, we identified nine SNVs in PD-1 (E84K, D85N, S87N, S87R, P89L, P89R, P89T, G90S, and G90V) affecting pembrolizumab but not nivolumab binding. Last, trastuzumab and pertuzumab, which bind different epitopes on the HER-2 antigen, were differentially affected by the $HER\text{-}2^{P594H}$ variant. Therefore, $HER\text{-}2^{P594H}$ carriers should not be treated with trastuzumab-derived products but rather pertuzumab-based products.

Although the clinical importance of the newly identified variants in our study remains to be elucidated, some prior clinical evidence supports personalization of mAb-based therapies. A key consideration is the need to contextualize these findings within global and population-specific datasets, given that some variants, although globally rare, may be more prevalent in certain populations. As an example, the $C5^{R885H}$ polymorphism is associated with poor response to eculizumab, a treatment for paroxysmal nocturnal hemoglobinuria (PNH). In the overall European population, this variant is rare (gnomADv4.1 allele frequency, 2.5×10^{-5}), but in the East Asian population, it reaches an allele frequency of 9.6×10^{-3}, with an estimated prevalence of ~3.5% in the Japanese population, similar among healthy individuals and patients with PNH (*21*). The clinical relevance of this variant is well documented. Among 345 treated patients with PNH, there were 11 nonresponders, all carrying the heterozygous $C5^{R885H}$ variant (*21*). Thus, even heterozygosity can be sufficient to cause therapy failure. Similarly, a patient with hematopoietic stem cell transplantation–associated thrombotic microangiopathy who

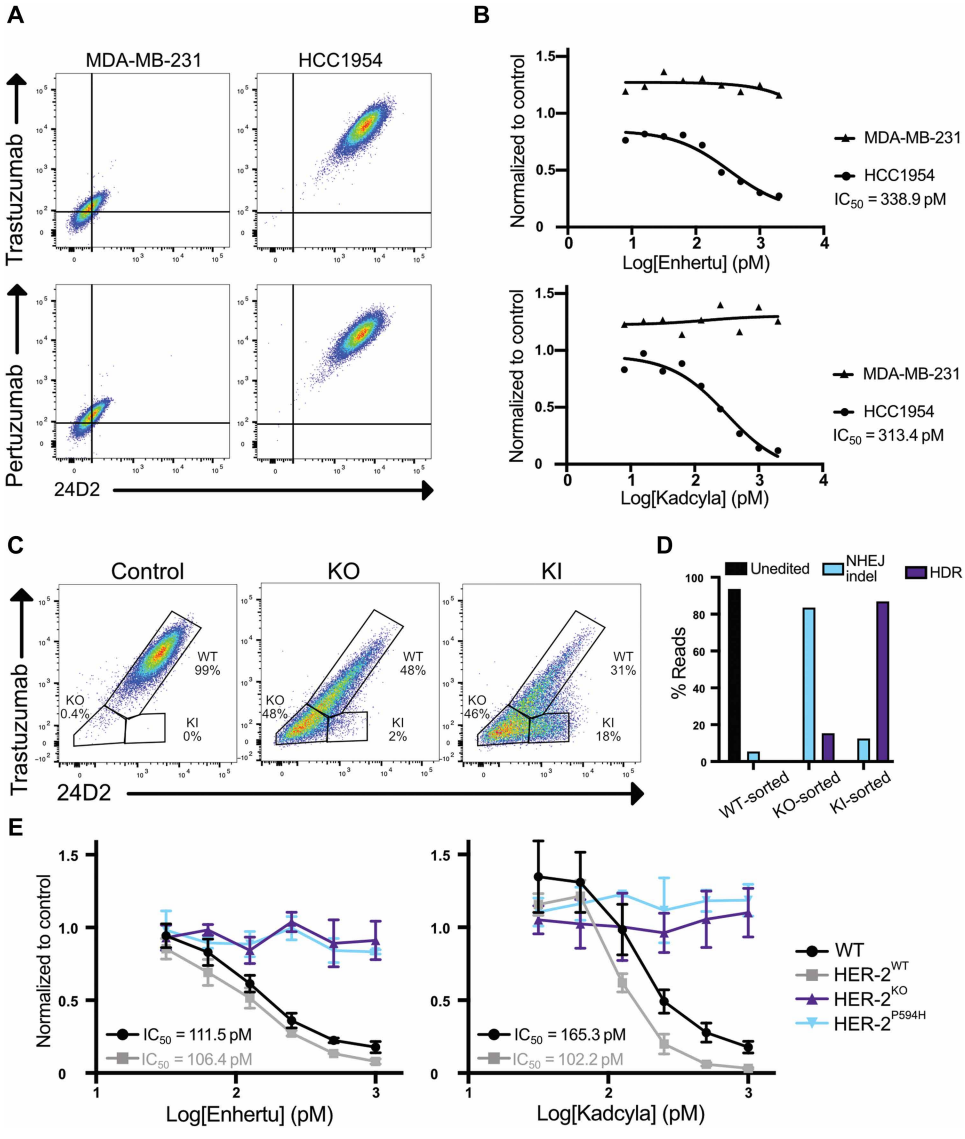

Fig. 7. Engineering the natural SNV HER-2^{P594H} in human breast tumor cells confers resistance to clinical ADCs. (**A**) Flow cytometry histograms show HER-2 expression in MDA-MB-231 and HCC1954 breast tumor cell lines. Staining was performed with HER-2 antibodies recognizing different epitopes (trastuzumab or pertuzumab combined with 24D2). (**B**) In vitro dose titration (killing curves) of Enhertu or Kadcyla applied to MDA-MB-231 and HCC1954 cells. (**C**) Flow cytometry plots show genome-edited HCC1954 cells 3 days after electroporation stained with HER-2 antibodies trastuzumab and 24D2. Control, cells electroporated with Cas9 protein only; KO, cells electroporated with Cas9 RNP; P594H, cells electroporated with Cas9 RNP and HDRT. In the flow cytometry histograms, double-positive cells are defined as WT, double-negative cells as KO, and cells binding only to clone 24D2 as KI. (**D**) Amplicon NGS of the targeted *ERBB2* locus after sorting of control, KO, and KI conditions. Unedited, WT codon; NHEJ/indel, indels at the Cas9 cutting site; HDR, KI codon and silent PAM mutation. (**E**) In vitro dose titration (killing curves) of Enhertu or Kadcyla applied to edited and sorted HCC1954 (WT-sorted, HER-2^{WT}; KO-sorted, HER-2^{KO}; KI-sorted, HER-2^{P594H}) and WT HCC1954 cells; data are presented as means ± SD. Data are normalized to untreated cells. For (A), $n = 2$ independent experiments for each group were performed. For (B) and (E), $n = 2$ or 3 independent experiments in triplicates for each group were performed. For (C), $n = 3$ independent experiments for each group were performed. For (D), $n = 1$ experiment was performed.

did not respond to eculizumab carried a C5^{R885H} variant. After switching to an alternative C5 inhibitor (Coversin), the patient initially improved but ultimately died because of limited Coversin supply (*53*). This emphasizes the importance of early identification of resistance-associated variants. Additional resistance variants, such as C5^{R885C} and C5^{R885S}, have been linked to reduced response or lack of efficacy with eculizumab, but switching to Coversin successfully treated one C5^{R885S} carrier patient (*54*). Similar to C5^{R885H}, these and other variants are present in our dataset and are predicted to affect eculizumab binding or antigen function, suggesting that computational predictions and experimental diagnostic tests should be considered for personalization of mAb treatments. In general, variants influencing antibody binding or antigen function can result in a range of resistance phenotypes, ranging from mild binding affinity changes to complete loss of binding. These effects may be mitigated by compensatory factors such as optimized dosing or alternative therapies (*55*). Therefore, germline epitope variants may account for some nonresponders to mAb therapies. In addition, secondary resistance could arise from somatic mutations acquired by target cells, as has been observed for CD19-directed CAR T therapy (*56*). In all cases, effective clinical management depends on early detection and characterization of resistance to enable timely and informed treatment decisions.

Our results show that multiple high-impact variants can be readily identified for most, if not all, antibodies and distinct SNVs will continuously be found. However, precise quantification of the impact remains challenging. Because computational methods and artificial intelligence continue to advance, they are expected to increasingly complement experimental approaches. Ultimately, the clinical relevance of variants also depends on their population frequency, which is unevenly documented. Here, we report it only for the experimentally validated cases. Therefore, we argue that truly individualized predictions of drug response, based on patients' genomic profiles, will require broader genetic variation coverage than is currently available to train accurate models. As noted, existing genetic studies often suffer from sparse data and population biases toward European ancestry in genomic data (*57*). Because genomic medicine and gene editing in medicine progress rapidly (*58*), human

genetic diversity becomes increasingly relevant for medical therapies (*59*–*61*). For example, a common genome variant in individuals of African ancestry creates an off-target site for the gRNA used in the first approved CRISPR-based therapy (*62*–*64*). Our findings underscore the need to capture global genetic diversity, given that broader and more diverse datasets may reveal additional polymorphisms affecting antigen-specific therapies or identify populations at higher risk of therapy failure (*65*). In such a scenario, antigen-specific immunotherapies may be customized to specific populations or even individuals. It is estimated that each individual's genome differs from the reference human genome at 4 to 5 million sites, with more than 99.9% of these differences being SNVs or short indels (*66*). Therefore, the variants annotated so far, as well as those analyzed here, represent only a fraction of the genetic variation that could affect antibody binding or treatment outcomes. Because large-scale genomic datasets continue to expand, our ability to capture epitope diversity is expected to improve accordingly.

The examples provided above, along with findings from pharmacogenomic studies, highlight the presence of actionable variants in the majority of genotyped patients (*67*). Because pharmacogenomics shifts from reactive testing of single genes to proactive multigene testing, preemptive testing may improve treatment efficacy, reduce adverse events, and lower costs for health care systems (*68*, *69*). In line with this, recent US Food and Drug Administration guidelines promote more comprehensive reporting of pharmacogenomic factors and initiatives to review gene-drug interactions (*70*). In this context, our study addresses a gap in the investigation of variants affecting mAb treatments, an area less explored compared with small-molecule drugs.

Our study is not without limitations. Computational methods provide a practical framework to estimate the structural and functional consequences of protein variants, but these methods do not always translate. Here, we used an empirical force field–based method (*24*, *71*) that has been extensively benchmarked (*72*) and whose application to mAb-Ag complexes is well documented (*26*, *73*–*77*). Our own experimental validation yielded comparable accuracy, further supporting its utility in this context (data file S3). However, the number of validated SNVs is limited, the fixed-backbone framework may limit accuracy in flexible loop regions, and our ground truth is based on a cell-based readout, rather than direct binding free energy measurements. Thus, these results serve as supportive evidence, rather than an independent assessment, of method performance. Because of these limitations, our computational predictions are best interpreted in conjunction with structural inspection and experimental validation. For the latter, we primarily validated predictions using research-grade biosimilars, but we also confirmed several predictions with clinically approved commercial products, including the clinical rituximab biosimilar Rixathon and the ADCs Kadcyla and Enhertu. Furthermore, because of lack of availability, we did not analyze cells or tissues from patients with primary treatment failure. The candidate SNVs identified here should be validated in future research, ideally in patient cohorts where samples are available before and after treatment.

Our findings have important implications for both clinical practice and therapeutic development. In particular, we argue that integrating genetic testing with accurate predictive models could help identify patients who are less likely to benefit from specific therapies. This has the potential to bring clarity for patients and physicians, reduce unnecessary treatments, minimize exposure to side effects, and optimize health care resources, ultimately improving patient care and outcomes. Moreover, our results may be valuable to the biotech and pharmaceutical industries. Accounting for genetic variation could help avoid false-negative outcomes that might otherwise bias clinical efficacy and could inform the development of mAbs targeting alternative, nonoverlapping epitopes, thereby enhancing treatment efficacy and coverage across genetically diverse patient groups.

MATERIALS AND METHODS

Study design

In this study, we investigated the impact of naturally occurring missense variants on mAb-Ag interactions and their potential role in driving resistance to antigen-specific therapies. Publicly available databases were accessed to retrieve antibody sequences, structural information about target antigens and therapeutic antibodies, and human genetic variants associated with the antigens. Computational analyses were then performed to estimate the potential effects of these variants on the stability of the antigens and antibody-antigen complexes. For experimental validation, representative examples were selected to include a diverse set of antigens expressed on both hematologic and nonhematologic cells. We chose antibody therapeutics with different mechanisms of action and with established clinical and commercial relevance. Computational predictions and experimental validation were done by different teams. Members of the experimental team were blinded for the flow cytometry expression experiments but not the killing experiment.

Dataset of therapeutic antibodies

Therapeutic antibody sequences were retrieved from the Thera-SabDab database (*78*), which catalogs antibody- and nanobody-based therapeutics recognized by the World Health Organization. Antibodies targeting human proteins with at least one experimental structure of the mAb-Ag complex were selected. The corresponding Protein Data Bank (PDB) files were renumbered using the Chothia scheme (*79*) by aligning heavy- and light-chain sequences to isotype-specific hidden Markov model profiles (*80*). The OpenStructure framework (*81*) was used to assess sequence identity between therapeutic sequences and the amino acid sequences of structural data, retaining only cases with 100% sequence identity. To exclude artifacts and distinguish biological interactions from crystallographic contacts, only structures with mAb-Ag interactions mediated by CDRs were retained. Antibodies with identical variable heavy- and light-chain amino acid sequences were clustered together, and a single representative was selected for analysis. The full list of antibodies analyzed in this study is provided in data file S1. Clinical trial status and therapeutic indications were manually curated using DrugBank (*82*), ClinicalTrials.gov, and the literature.

Human SNVs

The UniProt IDs of the protein targets (*83*) were used to query the European Bioinformatics Institute database by the Application Programming Interface (*84*) to retrieve a comprehensive collection of human genetic missense variants aggregated from multiple sources, including the Exome Aggregation Consortium (*85*), gnomAD (*86*), the 1000 Genomes Project (*66*), TopMed (*87*), ClinVar (*88*), The Cancer Genome Atlas (*89*), and COSMIC (*90*), along with disease annotation for the identified variants. Data were retrieved in October 2022.

From this dataset, only missense variants were retained for further analysis.

Computational analysis of SNV-associated amino acid variants

Variants were mapped onto the available 3D structures of mAb-Ag complexes using the Var3D variant annotation pipeline (version 1.3.0) available at (*91*). Epitopes were defined as the set of antigen residues within 5 Å to any residue of the antibody in the 3D complex. Sequence- and structure-related features for SNV-associated amino acid sites were computed by Var3D using the OpenStructure implementation (*81*). Specifically, per-residue relative solvent accessibility was computed using the NACCESS implementation of the Lee and Richards method (*92*). For each target sequence, an MSA was generated based on a Jackhammer search ($e < 1 \times 10^{-4}$) against the UniRef90 database (release 2021_04) (*93*, *94*). The resulting MSAs were used to compute Shannon entropy (*95*) and ConSurf conservation scores. $\Delta\Delta G$ values for each amino acid variant were computed using FoldX (*24*), with the 3D structure of the mAb-Ag complex and the isolated antigen structure as inputs. A $\Delta\Delta G$ cutoff of 1 kcal/mol was used to discriminate destabilizing mutations from neutral ones, consistent with the SD reported in the original validation of the method (*26*). AM (*25*) predictions were retrieved from (*96*). For validation purposes, both the predicted and experimentally observed effects on binding were binarized. Mutations were assigned a value of 1 if they affected binding and 0 otherwise. The correspondence between predictions and experimental observations was evaluated on the basis of accuracy, precision, and recall for a representative subset of variants in the dataset (data file S3).

Eukaryotic cell lines

UMNSAH/DF-1 cells were purchased from American Type Culture Collection (catalog no. CRL-12203) and were expanded in Dulbecco's modified Eagle's medium, high glucose (4.5 g/liter) (Sigma-Aldrich), supplemented with 10% fetal bovine serum (FBS) (Gibco Life Technologies) and 2 mM GlutaMAX (Gibco) at a temperature of 39°C. HCC1954 cells were a gift from M. Bentires-Alj (Department of Biomedicine, Basel, Switzerland) and were expanded in RPMI 1640 (Sigma-Aldrich) supplemented with 10% heat-inactivated FBS (Gibco Life Technologies) and 2 mM GlutaMAX. MDA-MB231 cells were a gift from M. Bentires-Alj and were expanded in Dulbecco's modified Eagle's medium, high glucose (4.5 g/liter) (Sigma-Aldrich), supplemented with 10% heat-inactivated FBS and 2 mM GlutaMAX.

Cloning and expression of various recombinant WT human genes and their variants

Full-length cDNAs of the genes encoding human CD20 (NM_021 950.3), human CD38 (NM_001775.2), human PD-1 (NM_005018.2), and human HER-2 (NM_004448.2) were obtained in a pCMV3 vector (catalog nos. HG11007-UT, HG10818-UT, HG10377-UT, and HG10004-UT, Sino Biological). The hygromycin sequence was replaced by a neomycin resistance cassette by restriction digestion. The SNVs of the human CD20, CD38, PD-1, and HER-2 variants selected for experimental validation were introduced into the cDNAs using the Q5 Site-Directed Mutagenesis Kit (catalog no. E055AS, New England Biolabs) (table S1).

A total of 1×10^6 UMNSAH/DF-1 cells were plated the day before transfection in a well of a six-well plate. The following day, the cells were transfected with 6.5 μg of DNA of the pCMV3 vector encoding WT cDNA or its variants and 19.5 μg of polyethyleneimine (catalog no. 23966, Polysciences) in 200 μl of serum free medium. Cells were incubated for 2 days at 39°C before further analysis.

Engineering of HCC1954 cell line

A total of 1×10^6 HCC1954 cells were resuspended in 20 μl of Lonza-supplemented SF electroporation buffer. Cas9 RNP complexes were freshly prepared as described before each electroporation (*18*). Thawed CRISPR RNA (crRNA) and transactivating crRNA (tracrRNA) (purchased from IDT Technologies; at 200 μM) were mixed in a 1:1 M ratio (120 pmol each), denatured at 95°C for 5 min, and annealed at room temperature for 10 min to complex an 80 μM gRNA solution. Polyglutamic acid (15 to 50 kDa at 100 mg/ml; Sigma-Aldrich) was added to the gRNA in a 0.8:1 volume ratio. To complex RNPs, 60 pmol of recombinant Cas9 (University of California Berkeley; at 40 μM) was mixed with the gRNA (molar ratio Cas9:gRNA = 1:2) and incubated for 20 min at room temperature. HDRT (purchased from IDT Technologies; 50 pmol) and RNPs (60 pmol) were mixed and incubated for 5 min. The cells were added to the mix, and the total volume was transferred to 16-well Nucleocuvette Strips. Electroporation was performed with the 4D-Nucleofector system (Lonza) with Program FF-150. Immediately following electroporation, 80 μl of prewarmed supplemented medium was added to each cuvette and incubated at 37°C. After 20 min, the cells were transferred into six-well culture plates containing 2 ml of medium. The HDRT contained the desired SNV and an additional silent mutation disrupting the PAM sequence to increase HDR efficiency. For crRNA and HDRT sequences, see table S2. Cells were cultured and expanded for flow cytometry analysis and cell sorting.

Flow cytometry and cell sorting

Unlabeled antibodies obtained from ProteoGenix and the Hospital Pharmacy were labeled using Alexa Fluor 647 *N*-hydroxysuccinimide (NHS) ester or Alexa Fluor 488 NHS ester, both from Thermo Fisher Scientific, following the manufacturer's instructions. Therapeutic antibodies are listed in Figs. 1B and 2C, table S3, and data file S1, whereas research control antibodies are listed only in table S3. Cells were collected and washed with FACS buffer consisting of phosphate-buffered saline (PBS) supplemented with 2% FBS. Subsequently, cells were stained with a fixable live/dead Zombie ultraviolet dye and blocked with a human Fc receptor binding reagent for 20 min at 4°C in PBS. After centrifugation, cells were stained with fluorophore-conjugated antibodies at room temperature for 30 min in FACS buffer. Flow cytometry was performed on a BD LSRFortessa with BD FACSDiva software. Data were analyzed with FlowJo software. For cell sorting, the HCC1954-engineered cells were pelleted, stained with HER-2 antibodies (clone 24D2 and trastuzumab), and resuspended in FACS buffer. The different populations were sorted on BD FACSAria running BD FACSDiva software directly into tubes containing FBS. After centrifugation, the different populations were expanded in RPMI 1640 supplemented with 10% heat-inactivated FBS, 2 mM GlutaMAX, and penicillin/streptomycin (100 IU/ml). A second cell sorting was performed in order to increase the purity of the sorted populations.

Genomic DNA extraction and NGS

Genomic DNA extraction was performed using QuickExtract (Lucigen). For NGS, a targeted amplicon library was prepared as three-step polymerase chain reaction protocol as previously described

(*16*) and paired-end sequenced on an Illumina MiniSeq instrument using the Illumina MiniSeq Mid output kit (300 cycles) with 50% PhiX spike-in (Illumina). The *ERBB2* locus was amplified using the primers listed in table S1. After demultiplexing, each sample was assessed for quality and processed using CRISPResso2 (*97*). Quantification of the different alleles (WT, KO, and KI) was performed using a custom script as previously described (*16*).

Killing assay

A total of 20,000 HCC1954 cells (WT, KO, and KI double sorted) were plated in 96-well plates in medium with corresponding concentrations of trastuzumab emtansine (Kadcyla) and trastuzumab deruxtecan (Enhertu) as described above. Following a 48-hour incubation period, cells were collected and stained for viability and with HER-2 antibodies (clone 24D2 and trastuzumab) as described above. Data were acquired on a BD LSRFortessa and analyzed with FlowJo.

Statistical analysis

Individual-level data for Fig. 7 are presented in data file S4. In Fig. 7 (B and E), IC_{50} (half-maximal inhibitory concentration) values were calculated. In Fig. 7E, data are presented as means ± SD, $n = 3$. In fig. S1, violin plots show the distributions of per-residue sequence entropy and relative solvent accessibility at antigen sites across the four SNV classes; overlaid box plots indicate the median and interquartile range.

Supplementary Materials

The PDF file includes:
Figs. S1 to S5
Tables S1 to S3
Legends for data files S1 to S4

Other Supplementary Material for this manuscript includes the following:
Data files S1 to S4
MDAR Reproducibility Checklist

REFERENCES AND NOTES

1. P. J. Carter, A. Rajpal, Designing antibodies as therapeutics. *Cell* **185**, 2789–2805 (2022).
2. S. E. Stark, A. J. Caton, Antibodies that are specific for a single amino acid interchange in a protein epitope use structurally distinct variable regions. *J. Exp. Med.* **174**, 613–624 (1991).
3. S. L. Zebedee, D. S. Barritt, W. C. Raschke, Comparison of mouse Ly5a and Ly5b leucocyte common antigen alleles. *Dev. Immunol.* **1**, 243–254 (1991).
4. A. Beck, T. Wurch, C. Bailly, N. Corvaia, Strategies and challenges for the next generation of therapeutic antibodies. *Nat. Rev. Immunol.* **10**, 345–352 (2010).
5. S. Paul, M. F. Konig, D. M. Pardoll, C. Bettegowda, N. Papadopoulos, K. M. Wright, S. B. Gabelli, M. Ho, A. van Elsas, S. Zhou, Cancer therapy with antibodies. *Nat. Rev. Cancer* **24**, 399–426 (2024).
6. M. E. Reff, K. Carner, K. S. Chambers, P. C. Chinn, J. E. Leonard, R. Raab, R. A. Newman, N. Hanna, D. R. Anderson, Depletion of B cells in vivo by a chimeric mouse human monoclonal antibody to CD20. *Blood* **83**, 435–445 (1994).
7. A. D. Gitlin, M. C. Nussenzweig, Immunology: Fifty years of B lymphocytes. *Nature* **517**, 139–141 (2015).
8. D. J. Slamon, B. Leyland-Jones, S. Shak, H. Fuchs, V. Paton, A. Bajamonde, T. Fleming, W. Eiermann, J. Wolter, M. Pegram, J. Baselga, L. Norton, Use of chemotherapy plus a monoclonal antibody against HER2 for metastatic breast cancer that overexpresses HER2. *N. Engl. J. Med.* **344**, 783–792 (2001).
9. A. Hoos, Development of immuno-oncology drugs - from CTLA4 to PD1 to the next generations. *Nat. Rev. Drug Discov.* **15**, 235–247 (2016).
10. S. M. Swain, M. Shastry, E. Hamilton, Targeting HER2-positive breast cancer: Advances and future directions. *Nat. Rev. Drug Discov.* **22**, 101–126 (2023).
11. R. Bargou, E. Leo, G. Zugmaier, M. Klinger, M. Goebeler, S. Knop, R. Noppeney, A. Viardot, G. Hess, M. Schuler, H. Einsele, C. Brandl, A. Wolf, P. Kirchinger, P. Klappers, M. Schmidt, G. Riethmuller, C. Reinhardt, P. A. Baeuerle, P. Kufer, Tumor regression in cancer patients by very low doses of a T cell-engaging antibody. *Science* **321**, 974–977 (2008).
12. A. F. Labrijn, M. L. Janmaat, J. M. Reichert, P. Parren, Bispecific antibodies: A mechanistic review of the pipeline. *Nat. Rev. Drug Discov.* **18**, 585–608 (2019).
13. C. H. June, M. Sadelain, Chimeric antigen receptor therapy. *N. Engl. J. Med.* **379**, 64–73 (2018).
14. B. L. Levine, M. C. Pasquini, J. E. Connolly, D. L. Porter, M. P. Gustafson, J. J. Boelens, E. M. Horwitz, S. A. Grupp, M. V. Maus, F. L. Locke, F. Ciceri, A. Ruggeri, J. Snowden, H. E. Heslop, C. L. Mackall, C. H. June, A. M. Sureda, M. A. Perales, Unanswered questions following reports of secondary malignancies after CAR-T cell therapy. *Nat. Med.* **30**, 338–341 (2024).
15. G. Casirati, A. Cosentino, A. Mucci, M. Salah Mahmoud, I. Ugarte Zabala, J. Zeng, S. B. Ficarro, D. Klatt, C. Brendel, A. Rambaldi, J. Ritz, J. A. Marto, D. Pellin, D. E. Bauer, S. A. Armstrong, P. Genovese, Epitope editing enables targeted immunotherapy of acute myeloid leukaemia. *Nature* **621**, 404–414 (2023).
16. S. Garaude, R. Marone, R. Lepore, A. Devaux, A. Beerlage, D. Seyres, A. Dell' Aglio, D. Juskevicius, J. Zuin, T. Burgold, S. Wang, V. Katta, G. Manquen, Y. Li, C. Larrue, A. Camus, I. Durzynska, L. C. Wellinger, I. Kirby, P. H. Van Berkel, C. Kunz, J. Tamburini, F. Bertoni, C. C. Widmer, S. Q. Tsai, F. Simonetta, S. Urlinger, L. T. Jeker, Selective haematological cancer eradication with preserved haematopoiesis. *Nature* **630**, 728–735 (2024).
17. M. Kornete, R. Marone, L. T. Jeker, Highly efficient and versatile plasmid-based gene editing in primary T cells. *J. Immunol.* **200**, 2489–2501 (2018).
18. R. Marone, E. Landmann, A. Devaux, R. Lepore, D. Seyres, J. Zuin, T. Burgold, C. Engdahl, G. Capoferri, A. Dell'Aglio, C. Larrue, F. Simonetta, J. Rositzka, M. Rhiel, G. Andrieux, D. N. Gallagher, M. S. Schroder, A. Wiederkehr, A. Sinopoli, V. Do Sacramento, A. Haydn, L. Garcia-Prat, C. Divsalar, A. Camus, L. Xu, L. Bordoli, T. Schwede, M. Porteus, J. Tamburini, J. E. Corn, T. Cathomen, T. I. Cornu, S. Urlinger, L. T. Jeker, Epitope-engineered human hematopoietic stem cells are shielded from CD123-targeted immunotherapy. *J. Exp. Med.* **220**, e20231235 (2023).
19. N. Wellhausen, R. P. O'Connell, S. Lesch, N. W. Engel, A. K. Rennels, D. Gonzales, F. Herbst, R. M. Young, K. C. Garcia, D. Weiner, C. H. June, S. I. Gill, Epitope base editing CD45 in hematopoietic cells enables universal blood cancer immune therapy. *Sci. Transl. Med.* **15**, eadi1145 (2023).
20. R. Marone, R. Lepore, J. Rositzka, V. Dettmer-Monaco, A. dell Aglio, G. Capoferri, J. Brault, E. Ten Buren, T. Burgold, A. Camus, C. Divsalar, L. Garcia Prat, A. Haydn, F. Hermann, M. Heugel, A. Knezevic, F. M. Lehmann, V. Do Sacramento, A. Sinopoli, L. C. Wellinger, A. Wiederkehr, S. Yumlu, T. Cathomen, T. Winkler, T. I. Cornu, D. Urlinger, L. T. Jeker, Function-preserving single amino acid substitutions shield hematopoietic stem and progenitor cells from CD117 targeted immunotherapy in vivo. *Blood* **140**, 4493–4494 (2022).
21. J. Nishimura, M. Yamamoto, S. Hayashi, K. Ohyashiki, K. Ando, A. L. Brodsky, H. Noji, K. Kitamura, T. Eto, T. Takahashi, M. Masuko, T. Matsumoto, Y. Wano, T. Shichishima, H. Shibayama, M. Hase, L. Li, K. Johnson, A. Lazarowski, P. Tamburini, J. Inazawa, T. Kinoshita, Y. Kanakura, Genetic variants in C5 and poor response to eculizumab. *N. Engl. J. Med.* **370**, 632–639 (2014).
22. X. Lyu, Q. Zhao, J. Hui, T. Wang, M. Lin, K. Wang, J. Zhang, J. Shentu, P. A. Dalby, H. Zhang, B. Liu, The global landscape of approved antibody therapies. *Antib. Ther.* **5**, 233–257 (2022).
23. A. Mullard, FDA approves 100th monoclonal antibody product. *Nat. Rev. Drug Discov.* **20**, 491–495 (2021).
24. J. Schymkowitz, J. Borg, F. Stricher, R. Nys, F. Rousseau, L. Serrano, The FoldX web server: An online force field. *Nucleic Acids Res.* **33**, W382–W388 (2005).
25. J. Cheng, G. Novati, J. Pan, C. Bycroft, A. Zemgulyte, T. Applebaum, A. Pritzel, L. H. Wong, M. Zielinski, T. Sargeant, R. G. Schneider, A. W. Senior, J. Jumper, D. Hassabis, P. Kohli, Z. Avsec, Accurate proteome-wide missense variant effect prediction with AlphaMissense. *Science* **381**, eadg7492 (2023).
26. R. Guerois, J. E. Nielsen, L. Serrano, Predicting changes in the stability of proteins and protein complexes: A study of more than 1000 mutations. *J. Mol. Biol.* **320**, 369–387 (2002).
27. M. de Weers, Y. T. Tai, M. S. van der Veer, J. M. Bakker, T. Vink, D. C. Jacobs, L. A. Oomen, M. Peipp, T. Valerius, J. W. Slootstra, T. Mutis, W. K. Bleeker, K. C. Anderson, H. M. Lokhorst, J. G. van de Winkel, P. W. Parren, Daratumumab, a novel therapeutic human CD38 monoclonal antibody, induces killing of multiple myeloma and other hematological tumors. *J. Immunol.* **186**, 1840–1848 (2011).
28. M. J. E. Marshall, R. J. Stopforth, M. S. Cragg, Therapeutic antibodies: What have we learnt from targeting CD20 and where are we going? *Front. Immunol.* **8**, 1245 (2017).
29. T. van Meerten, A. Hagenbeek, CD20-targeted therapy: The next generation of antibodies. *Semin. Hematol.* **47**, 199–210 (2010).
30. L. Rouge, N. Chiang, M. Steffek, C. Kugel, T. I. Croll, C. Tam, A. Estevez, C. P. Arthur, C. M. Koth, C. Ciferri, E. Kraft, J. Payandeh, G. Nakamura, J. T. Koerber, A. Rohou, Structure

of CD20 in complex with the therapeutic monoclonal antibody rituximab. *Science* **367**, 1224–1230 (2020).
31. S. O'Brien, A. Osterborg, Ofatumumab: A new CD20 monoclonal antibody therapy for B-cell chronic lymphocytic leukemia. *Clin. Lymphoma Myeloma Leuk.* **10**, 361–368 (2010).
32. A. W. Pawluczkowycz, F. J. Beurskens, P. V. Beum, M. A. Lindorfer, J. G. van de Winkel, P. W. Parren, R. P. Taylor, Binding of submaximal C1q promotes complement-dependent cytotoxicity (CDC) of B cells opsonized with anti-CD20 mAbs ofatumumab (OFA) or rituximab (RTX): Considerably higher levels of CDC are induced by OFA than by RTX. *J. Immunol.* **183**, 749–758 (2009).
33. J. Du, H. Wang, C. Zhong, B. Peng, M. Zhang, B. Li, S. Hou, Y. Guo, J. Ding, Crystal structure of chimeric antibody C2H7 Fab in complex with a CD20 peptide. *Mol. Immunol.* **45**, 2861–2868 (2008).
34. J. Du, H. Wang, C. Zhong, B. Peng, M. Zhang, B. Li, S. Huo, Y. Guo, J. Ding, Structural basis for recognition of CD20 by therapeutic antibody rituximab. *J. Biol. Chem.* **282**, 15073–15080 (2007).
35. J. Du, H. Yang, Y. Guo, J. Ding, Structure of the Fab fragment of therapeutic antibody ofatumumab provides insights into the recognition mechanism with CD20. *Mol. Immunol.* **46**, 2419–2423 (2009).
36. F. Shen, W. Shen, Isatuximab in the treatment of multiple myeloma: A review and comparison with daratumumab. *Technol. Cancer Res. Treat.* **21**, 15330338221106563 (2022).
37. J. Deckert, M. C. Wetzel, L. M. Bartle, A. Skaletskaya, V. S. Goldmacher, F. Vallee, Q. Zhou-Liu, P. Ferrari, S. Pouzieux, C. Lahoute, C. Dumontet, A. Plesa, M. Chiron, P. Lejeune, T. Chittenden, P. U. Park, V. Blanc, SAR650984, a novel humanized CD38-targeting antibody, demonstrates potent antitumor activity in models of multiple myeloma and other $CD38^+$ hematologic malignancies. *Clin. Cancer Res.* **20**, 4574–4583 (2014).
38. H. T. Lee, Y. Kim, U. B. Park, T. J. Jeong, S. H. Lee, Y. S. Heo, Crystal structure of CD38 in complex with daratumumab, a first-in-class anti-CD38 antibody drug for treating multiple myeloma. *Biochem. Biophys. Res. Commun.* **536**, 26–31 (2021).
39. Y. Iwai, M. Ishida, Y. Tanaka, T. Okazaki, T. Honjo, N. Minato, Involvement of PD-L1 on tumor cells in the escape from host immune system and tumor immunotherapy by PD-L1 blockade. *Proc. Natl. Acad. Sci. U.S.A.* **99**, 12293–12297 (2002).
40. A. Ribas, J. D. Wolchok, Cancer immunotherapy using checkpoint blockade. *Science* **359**, 1350–1355 (2018).
41. A. H. Sharpe, K. E. Pauken, The diverse functions of the PD1 inhibitory pathway. *Nat. Rev. Immunol.* **18**, 153–167 (2018).
42. H. S. Cho, K. Mason, K. X. Ramyar, A. M. Stanley, S. B. Gabelli, D. W. Denney Jr., D. J. Leahy, Structure of the extracellular region of HER2 alone and in complex with the Herceptin Fab. *Nature* **421**, 756–760 (2003).
43. J. Albanell, J. Codony, A. Rovira, B. Mellado, P. Gascon, Mechanism of action of anti-HER2 monoclonal antibodies: Scientific update on trastuzumab and 2C4. *Adv. Exp. Med. Biol.* **532**, 253–268 (2003).
44. A. H. Boekhout, J. H. Beijnen, J. H. Schellens, Trastuzumab. *Oncologist* **16**, 800–810 (2011).
45. J. Cortes, S. B. Kim, W. P. Chung, S. A. Im, Y. H. Park, R. Hegg, M. H. Kim, L. M. Tseng, V. Petry, C. F. Chung, H. Iwata, E. Hamilton, G. Curigliano, B. Xu, C. S. Huang, J. H. Kim, J. W. Y. Chiu, J. L. Pedrini, C. Lee, Y. Liu, J. Cathcart, E. Bako, S. Verma, S. A. Hurvitz, DESTINY-Breast03 Trial Investigators, Trastuzumab deruxtecan versus trastuzumab emtansine for breast cancer. *N. Engl. J. Med.* **386**, 1143–1154 (2022).
46. M. C. Franklin, K. D. Carey, F. F. Vajdos, D. J. Leahy, A. M. de Vos, M. X. Sliwkowski, Insights into ErbB signaling from the structure of the ErbB2-pertuzumab complex. *Cancer Cell* **5**, 317–328 (2004).
47. W. Scheuer, T. Friess, H. Burtscher, B. Bossenmaier, J. Endl, M. Hasmann, Strongly enhanced antitumor activity of trastuzumab and pertuzumab combination treatment on HER2-positive human xenograft tumor models. *Cancer Res.* **69**, 9330–9336 (2009).
48. M. Senior, Cancer-targeting antibody-drug conjugates drive dealmaking frenzy. *Nat. Biotechnol.* **42**, 362–366 (2024).
49. Y. Zhu, K. Liu, K. Wang, H. Zhu, Treatment-related adverse events of antibody-drug conjugates in clinical trials: A systematic review and meta-analysis. *Cancer* **129**, 283–295 (2023).
50. H. Saber, J. K. Leighton, An FDA oncology analysis of antibody-drug conjugates. *Regul. Toxicol. Pharmacol.* **71**, 444–452 (2015).
51. H. Saber, N. Simpson, T. K. Ricks, J. K. Leighton, An FDA oncology analysis of toxicities associated with PBD-containing antibody-drug conjugates. *Regul. Toxicol. Pharmacol.* **107**, 104429 (2019).
52. R. Colombo, J. R. Rich, The therapeutic window of antibody drug conjugates: A dogma in need of revision. *Cancer Cell* **40**, 1255–1263 (2022).
53. T. H. J. Goodship, F. Pinto, W. H. Weston-Davies, J. Silva, J. I. Nishimura, M. A. Nunn, I. Mackie, S. J. Machin, L. Palm, J. W. Pryce, R. Chiesa, P. Amrolia, P. Veys, Use of the complement inhibitor Coversin to treat HSCT-associated TMA. *Blood Adv.* **1**, 1254–1258 (2017).
54. S. Schols, M. A. Nunn, I. Mackie, W. Weston-Davies, J. I. Nishimura, Y. Kanakura, N. Blijlevens, P. Muus, S. Langemeijer, Successful treatment of a PNH patient non-responsive to eculizumab with the novel complement C5 inhibitor coversin (nomacopan). *Br. J. Haematol.* **188**, 334–337 (2020).
55. H. B. Bouwman, H. J. Guchelaar, The efficacy and safety of eculizumab in patients and the role of C5 polymorphisms. *Drug Discov. Today* **29**, 104134 (2024).
56. E. Sotillo, D. M. Barrett, K. L. Black, A. Bagashev, D. Oldridge, G. Wu, R. Sussman, C. Lanauze, M. Ruella, M. R. Gazzara, N. M. Martinez, C. T. Harrington, E. Y. Chung, J. Perazzelli, T. J. Hofmann, S. L. Maude, P. Raman, A. Barrera, S. Gill, S. F. Lacey, J. J. Melenhorst, D. Allman, E. Jacoby, T. Fry, C. Mackall, Y. Barash, K. W. Lynch, J. M. Maris, S. A. Grupp, A. Thomas-Tikhonenko, Convergence of acquired mutations and alternative splicing of CD19 enables resistance to CART-19 immunotherapy. *Cancer Discov.* **5**, 1282–1295 (2015).
57. A. B. Popejoy, S. M. Fullerton, Genomics is failing on diversity. *Nature* **538**, 161–164 (2016).
58. G. Q. Daley, Welcoming the era of gene editing in medicine. *N. Engl. J. Med.* **390**, 1642–1645 (2024).
59. D. A. Scott, F. Zhang, Implications of human genetic variation in CRISPR-based therapeutic genome editing. *Nat. Med.* **23**, 1095–1101 (2017).
60. L. Yang, D. Grishin, G. Wang, J. Aach, C. Z. Zhang, R. Chari, J. Homsy, X. Cai, Y. Zhao, J. B. Fan, C. Seidman, J. Seidman, W. Pu, G. Church, Targeted and genome-wide sequencing reveal single nucleotide variations impacting specificity of Cas9 in human stem cells. *Nat. Commun.* **5**, 5507 (2014).
61. C. R. Lazzarotto, Y. Li, A. R. Flory, J. Chyr, M. Yang, V. Katta, E. Urbina, G. Lee, R. Wood, A. Matsubara, S. R. Rashkin, J. Ma, Y. Cheng, S. Q. Tsai, Population-scale cellular GUIDE-seq-2 and biochemical CHANGE-seq-R profiles reveal human genetic variation frequently affects Cas9 off-target activity. bioRxiv 2025.02.10.637517 [Preprint] (2025); https://doi.org/10.1101/2025.02.10.637517.
62. H. Frangoul, F. Locatelli, A. Sharma, M. Bhatia, M. Mapara, L. Molinari, D. Wall, R. I. Liem, P. Telfer, A. J. Shah, M. Cavazzana, S. Corbacioglu, D. Rondelli, R. Meisel, L. Dedeken, S. Lobitz, M. de Montalembert, M. H. Steinberg, M. C. Walters, M. J. Eckrich, S. Imren, L. Bower, C. Simard, W. Zhou, F. Xuan, P. K. Morrow, W. E. Hobbs, S. A. Grupp, CLIMB SCD-121 Study Group, Exagamglogene autotemcel for severe sickle cell disease. *N. Engl. J. Med.* **390**, 1649–1662 (2024).
63. F. Locatelli, P. Lang, D. Wall, R. Meisel, S. Corbacioglu, A. M. Li, J. de la Fuente, A. J. Shah, B. Carpenter, J. L. Kwiatkowski, M. Mapara, R. I. Liem, M. D. Cappellini, M. Algeri, A. Kattamis, S. Sheth, S. Grupp, R. Handgretinger, P. Kohli, D. Shi, L. Ross, Y. Bobruff, C. Simard, L. Zhang, P. K. Morrow, W. E. Hobbs, H. Frangoul, CLIMB THAL-111 Study Group, Exagamglogene autotemcel for transfusion-dependent β-thalassemia. *N. Engl. J. Med.* **390**, 1663–1676 (2024).
64. S. Cancellieri, J. Zeng, L. Y. Lin, M. Tognon, M. A. Nguyen, J. Lin, N. Bombieri, S. A. Maitland, M. F. Ciuculescu, V. Katta, S. Q. Tsai, M. Armant, S. A. Wolfe, R. Giugno, D. E. Bauer, L. Pinello, Human genetic diversity alters off-target outcomes of therapeutic gene editing. *Nat. Genet.* **55**, 34–43 (2023).
65. A. Verma, J. E. Huffman, A. Rodriguez, M. Conery, M. Liu, Y. L. Ho, Y. Kim, D. A. Heise, L. Guare, V. A. Panickan, H. Garcon, F. Linares, L. Costa, I. Goethert, R. Tipton, J. Honerlaw, L. Davies, S. Whitbourne, J. Cohen, D. C. Posner, R. Sangar, M. Murray, X. Wang, D. R. Dochtermann, P. Devineni, Y. Shi, T. N. Nandi, T. L. Assimes, C. A. Brunette, R. J. Carroll, R. Clifford, S. Duvall, J. Gelernter, A. Hung, S. K. Iyengar, J. Joseph, R. Kember, H. Kranzler, C. M. Kripke, D. Levey, S. W. Luoh, V. C. Merritt, C. Overstreet, J. D. Deak, S. F. A. Grant, R. Polimanti, P. Roussos, G. Shakt, Y. V. Sun, N. Tsao, S. Venkatesh, G. Voloudakis, A. Justice, E. Begoli, R. Ramoni, G. Tourassi, S. Pyarajan, P. Tsao, C. J. O'Donnell, S. Muralidhar, J. Moser, J. P. Casas, A. G. Bick, W. Zhou, T. Cai, B. F. Voight, K. Cho, J. M. Gaziano, R. K. Madduri, S. Damrauer, K. P. Liao, Diversity and scale: Genetic architecture of 2068 traits in the VA million veteran program. *Science* **385**, eadj1182 (2024).
66. The 1000 Genomes Project Consortium, A global reference for human genetic variation. *Nature* **526**, 68–74 (2015).
67. S. L. Van Driest, Y. Shi, E. A. Bowton, J. S. Schildcrout, J. F. Peterson, J. Pulley, J. C. Denny, D. M. Roden, Clinically actionable genotypes among 10,000 patients with preemptive pharmacogenomic testing. *Clin. Pharmacol. Ther.* **95**, 423–431 (2014).
68. K. Krebs, L. Milani, Translating pharmacogenomics into clinical decisions: Do not let the perfect be the enemy of the good. *Hum. Genomics* **13**, 39 (2019).
69. M. Pirmohamed, G. Burnside, N. Eriksson, A. L. Jorgensen, C. H. Toh, T. Nicholson, P. Kesteven, C. Christersson, B. Wahlstrom, C. Stafberg, J. E. Zhang, J. B. Leathart, H. Kohnke, A. H. M. van der Zee, P. R. Williamson, A. K. Daly, P. Avery, F. Kamali, M. Wadelius, EU-PACT Group, A randomized trial of genotype-guided dosing of warfarin. *N. Engl. J. Med.* **369**, 2294–2303 (2013).
70. US Food and Drug Administration, "Table of Pharmacogenetic Associations," 26 October 2022; www.fda.gov/medical-devices/precision-medicine/table-pharmacogenetic-associations.
71. J. Mendes, R. Guerois, L. Serrano, Energy estimation in protein design. *Curr. Opin. Struct. Biol.* **12**, 441–446 (2002).
72. O. Buss, J. Rudat, K. Ochsenreither, FoldX as protein engineering tool: Better than random based approaches? *Comput. Struct. Biotechnol. J.* **16**, 25–33 (2018).

73. S. Sirin, J. R. Apgar, E. M. Bennett, A. E. Keating, AB-Bind: Antibody binding mutational database for computational affinity predictions. *Protein Sci.* **25**, 393–409 (2016).
74. J. E. Barnes, P. K. Lund-Andersen, J. S. Patel, F. M. Ytreberg, The effect of mutations on binding interactions between the SARS-CoV-2 receptor binding domain and neutralizing antibodies B38 and CB6. *Sci. Rep.* **12**, 18819 (2022).
75. L. A. Chi, J. E. Barnes, J. S. Patel, F. M. Ytreberg, Exploring the ability of the MD+FoldX method to predict SARS-CoV-2 antibody escape mutations using large-scale data. *Sci. Rep.* **14**, 23122 (2024).
76. A. M. Hummer, C. Schneider, L. Chinery, C. M. Deane, Investigating the volume and diversity of data needed for generalizable antibody-antigen ΔΔG prediction. *Nat. Comput. Sci.* **5**, 635–647 (2025).
77. B. Janusz, D. Chomicz, S. Demharter, M. Arts, J. de Kanter, Y. Wilke, H. Britze, S. Wrobel, T. Gawłowski, P. Dudzic, K. Ukkivi, L. Peil, R. Spreafico, K. Krawczyk, AbDesign: Database of point mutants of antibodies with associated structures reveals poor generalization of binding predictions from machine learning models. *MAbs* **17**, 2567319 (2025).
78. M. I. J. Raybould, C. Marks, A. P. Lewis, J. Shi, A. Bujotzek, B. Taddese, C. M. Deane, Thera-SAbDab: The therapeutic structural antibody database. *Nucleic Acids Res.* **48**, D383–D388 (2020).
79. C. Chothia, A. M. Lesk, Canonical structures for the hypervariable regions of immunoglobulins. *J. Mol. Biol.* **196**, 901–917 (1987).
80. R. Lepore, P. P. Olimpieri, M. A. Messih, A. Tramontano, PIGSPro: Prediction of immunoGlobulin structures v2. *Nucleic Acids Res.* **45**, W17–W23 (2017).
81. M. Biasini, T. Schmidt, S. Bienert, V. Mariani, G. Studer, J. Haas, N. Johner, A. D. Schenk, A. Philippsen, T. Schwede, OpenStructure: An integrated software framework for computational structural biology. *Acta Crystallogr. D Biol. Crystallogr.* **69**, 701–709 (2013).
82. D. S. Wishart, Y. D. Feunang, A. C. Guo, E. J. Lo, A. Marcu, J. R. Grant, T. Sajed, D. Johnson, C. Li, Z. Sayeeda, N. Assempour, I. Iynkkaran, Y. Liu, A. Maciejewski, N. Gale, A. Wilson, L. Chin, R. Cummings, D. Le, A. Pon, C. Knox, M. Wilson, DrugBank 5.0: A major update to the DrugBank database for 2018. *Nucleic Acids Res.* **46**, D1074–D1082 (2018).
83. C. UniProt, UniProt: The universal protein knowledgebase in 2023. *Nucleic Acids Res.* **51**, D523–D531 (2023).
84. F. Madeira, M. Pearce, A. R. N. Tivey, P. Basutkar, J. Lee, O. Edbali, N. Madhusoodanan, A. Kolesnikov, R. Lopez, Search and sequence analysis tools services from EMBL-EBI in 2022. *Nucleic Acids Res.* **50**, W276–W279 (2022).
85. M. Lek, K. J. Karczewski, E. V. Minikel, K. E. Samocha, E. Banks, T. Fennell, A. H. O'Donnell-Luria, J. S. Ware, A. J. Hill, B. B. Cummings, T. Tukiainen, D. P. Birnbaum, J. A. Kosmicki, L. E. Duncan, K. Estrada, F. Zhao, J. Zou, E. Pierce-Hoffman, J. Berghout, D. N. Cooper, N. Deflaux, M. DePristo, R. Do, J. Flannick, M. Fromer, L. Gauthier, J. Goldstein, N. Gupta, D. Howrigan, A. Kiezun, M. I. Kurki, A. L. Moonshine, P. Natarajan, L. Orozco, G. M. Peloso, R. Poplin, M. A. Rivas, V. Ruano-Rubio, S. A. Rose, D. M. Ruderfer, K. Shakir, P. D. Stenson, C. Stevens, B. P. Thomas, G. Tiao, M. T. Tusie-Luna, B. Weisburd, H. H. Won, D. Yu, D. M. Altshuler, D. Ardissino, M. Boehnke, J. Danesh, S. Donnelly, R. Elosua, J. C. Florez, S. B. Gabriel, G. Getz, S. J. Glatt, C. M. Hultman, S. Kathiresan, M. Laakso, S. McCarroll, M. I. McCarthy, D. McGovern, R. McPherson, B. M. Neale, A. Palotie, S. M. Purcell, D. Saleheen, J. M. Scharf, P. Sklar, P. F. Sullivan, J. Tuomilehto, M. T. Tsuang, H. C. Watkins, J. G. Wilson, M. J. Daly, D. G. MacArthur, Exome Aggregation Consortium, Analysis of protein-coding genetic variation in 60,706 humans. *Nature* **536**, 285–291 (2016).
86. K. J. Karczewski, L. C. Francioli, G. Tiao, B. B. Cummings, J. Alfoldi, Q. Wang, R. L. Collins, K. M. Laricchia, A. Ganna, D. P. Birnbaum, L. D. Gauthier, H. Brand, M. Solomonson, N. A. Watts, D. Rhodes, M. Singer-Berk, E. M. England, E. G. Seaby, J. A. Kosmicki, R. K. Walters, K. Tashman, Y. Farjoun, E. Banks, T. Poterba, A. Wang, C. Seed, N. Whiffin, J. X. Chong, K. E. Samocha, E. Pierce-Hoffman, Z. Zappala, A. H. O'Donnell-Luria, E. V. Minikel, B. Weisburd, M. Lek, J. S. Ware, C. Vittal, I. M. Armean, L. Bergelson, K. Cibulskis, K. M. Connolly, M. Covarrubias, S. Donnelly, S. Ferriera, S. Gabriel, J. Gentry, N. Gupta, T. Jeandet, D. Kaplan, C. Llanwarne, R. Munshi, S. Novod, N. Petrillo, D. Roazen, V. Ruano-Rubio, A. Saltzman, M. Schleicher, J. Soto, K. Tibbetts, C. Tolonen, G. Wade, M. E. Talkowski, Genome Aggregation Database Consortium, B. M. Neale, M. J. Daly, D. G. MacArthur, The mutational constraint spectrum quantified from variation in 141,456 humans. *Nature* **581**, 434–443 (2020).
87. D. Taliun, D. N. Harris, M. D. Kessler, J. Carlson, Z. A. Szpiech, R. Torres, S. A. G. Taliun, A. Corvelo, S. M. Gogarten, H. M. Kang, A. N. Pitsillides, J. LeFaive, S. B. Lee, X. Tian, B. L. Browning, S. Das, A. K. Emde, W. E. Clarke, D. P. Loesch, A. C. Shetty, T. W. Blackwell, A. V. Smith, Q. Wong, X. Liu, M. P. Conomos, D. M. Bobo, F. Aguet, C. Albert, A. Alonso, K. G. Ardlie, D. E. Arking, S. Aslibekyan, P. L. Auer, J. Barnard, R. G. Barr, L. Barwick, L. C. Becker, R. L. Beer, E. J. Benjamin, L. F. Bielak, J. Blangero, M. Boehnke, D. W. Bowden, J. A. Brody, E. G. Burchard, B. E. Cade, J. F. Casella, B. Chalazan, D. I. Chasman, Y. I. Chen, M. H. Cho, S. H. Choi, M. K. Chung, C. B. Clish, A. Correa, J. E. Curran, B. Custer, D. Darbar, M. Daya, M. de Andrade, D. L. DeMeo, S. K. Dutcher, P. T. Ellinor, L. S. Emery, C. Eng, D. Fatkin, T. Fingerlin, L. Forer, M. Fornage, N. Franceschini, C. Fuchsberger, S. M. Fullerton, S. Germer, M. T. Gladwin, D. J. Gottlieb, X. Guo, M. E. Hall, J. He, N. L. Heard-Costa, S. R. Heckbert, M. R. Irvin, J. M. Johnsen, A. D. Johnson, R. Kaplan, S. L. R. Kardia, T. Kelly, S. Kelly, E. E. Kenny, D. P. Kiel, R. Klemmer, B. A. Konkle, C. Kooperberg, A. Kottgen, L. A. Lange, J. Lasky-Su, D. Levy, X. Lin, K. H. Lin, C. Liu, R. J. F. Loos, L. Garman, R. Gerszten, S. A. Lubitz, K. L. Lunetta, A. C. Y. Mak, A. Manichaikul, A. K. Manning, R. A. Mathias, D. D. McManus, S. T. McGarvey, J. B. Meigs, D. A. Meyers, J. L. Mikulla, M. A. Minear, B. D. Mitchell, S. Mohanty, M. E. Montasser, C. Montgomery, A. C. Morrison, J. M. Murabito, A. Natale, P. Natarajan, S. C. Nelson, K. E. North, J. R. O'Connell, N. D. Palmer, N. Pankratz, G. M. Peloso, P. A. Peyser, J. Pleiness, W. S. Post, B. M. Psaty, D. C. Rao, S. Redline, A. P. Reiner, D. Roden, J. I. Rotter, I. Ruczinski, C. Sarnowski, S. Schoenherr, D. A. Schwartz, J. S. Seo, S. Seshadri, V. A. Sheehan, W. H. Sheu, M. B. Shoemaker, N. L. Smith, J. A. Smith, N. Sotoodehnia, A. M. Stilp, W. Tang, K. D. Taylor, M. Telen, T. A. Thornton, R. P. Tracy, D. J. Van Den Berg, R. S. Vasan, K. A. Viaud-Martinez, S. Vrieze, D. E. Weeks, B. S. Weir, S. T. Weiss, L. C. Weng, C. J. Willer, Y. Zhang, X. Zhao, D. K. Arnett, A. E. Ashley-Koch, K. C. Barnes, E. Boerwinkle, S. Gabriel, R. Gibbs, K. M. Rice, S. S. Rich, E. K. Silverman, P. Qasba, W. Gan, NHLBI Trans-Omics for Precision Medicine (TOPMed) Consortium, G. J. Papanicolaou, D. A. Nickerson, S. R. Browning, M. C. Zody, S. Zollner, J. G. Wilson, L. A. Cupples, C. C. Laurie, C. E. Jaquish, R. D. Hernandez, T. D. O'Connor, G. R. Abecasis, Sequencing of 53,831 diverse genomes from the NHLBI TOPMed Program. *Nature* **590**, 290–299 (2021).
88. M. J. Landrum, S. Chitipiralla, G. R. Brown, C. Chen, B. Gu, J. Hart, D. Hoffman, W. Jang, K. Kaur, C. Liu, V. Lyoshin, Z. Maddipatla, R. Maiti, J. Mitchell, N. O'Leary, G. R. Riley, W. Shi, G. Zhou, V. Schneider, D. Maglott, J. B. Holmes, B. L. Kattman, ClinVar: Improvements to accessing data. *Nucleic Acids Res.* **48**, D835–D844 (2020).
89. The Cancer Genome Atlas Research Network, J. N. Weinstein, E. A. Collisson, G. B. Mills, K. R. Shaw, B. A. Ozenberger, K. Ellrott, I. Shmulevich, C. Sander, J. M. Stuart, The cancer genome atlas pan-cancer analysis project. *Nat. Genet.* **45**, 1113–1120 (2013).
90. J. G. Tate, S. Bamford, H. C. Jubb, Z. Sondka, D. M. Beare, N. Bindal, H. Boutselakis, C. G. Cole, C. Creatore, E. Dawson, P. Fish, B. Harsha, C. Hathaway, S. C. Jupe, C. Y. Kok, K. Noble, L. Ponting, C. C. Ramshaw, C. E. Rye, H. E. Speedy, R. Stefancsik, S. L. Thompson, S. Wang, S. Ward, P. J. Campbell, S. A. Forbes, COSMIC: The catalogue of somatic mutations in cancer. *Nucleic Acids Res.* **47**, D941–D947 (2019).
91. schwede, "var3d," GitHub (2022); https://git.scicore.unibas.ch/schwede/var3d.
92. B. Lee, F. M. Richards, The interpretation of protein structures: Estimation of static accessibility. *J. Mol. Biol.* **55**, 379–400 (1971).
93. S. R. Eddy, Accelerated profile HMM searches. *PLoS Comput. Biol.* **7**, e1002195 (2011).
94. B. E. Suzek, Y. Wang, H. Huang, P. B. McGarvey, C. H. Wu, C. UniProt, UniRef clusters: A comprehensive and scalable alternative for improving sequence similarity searches. *Bioinformatics* **31**, 926–932 (2015).
95. C. E. Shannon, A mathematical theory of communication. *Bell Syst. Tech. J.* **27**, 379–423 (1948).
96. Google Cloud, dm_alphamissense; https://console.cloud.google.com/storage/browser/dm_alphamissense.
97. K. Clement, H. Rees, M. C. Canver, J. M. Gehrke, R. Farouni, J. Y. Hsu, M. A. Cole, D. R. Liu, J. K. Joung, D. E. Bauer, L. Pinello, CRISPResso2 provides accurate and rapid genome editing sequence analysis. *Nat. Biotechnol.* **37**, 224–226 (2019).

Acknowledgments: HCC1954 and MDA-MB-231 cell lines were a gift of M. Bentires-Alj. Clinical ADCs were a gift of N. Ott and the Pharmacy of the University Hospital Basel. We acknowledge the flow cytometry facility at the University of Basel and the Department of Biomedicine for support. Calculations were performed at sciCORE (http://scicore.unibas.ch/) scientific computing center at University of Basel. We thank G. Studer for assistance with the GitHub distribution of the Var3D pipeline and V. Senn for experimental support. **Funding:** This project has received funding from the European Research Council (ERC) under the European Union's Horizon 2020 research and innovation programme (grant agreement 818806 to L.T.J.) and institutional funds by the Department of Biomedicine. T.S. and E.A. acknowledge support by the SIB Swiss Institute of Bioinformatics and the Department Biozentrum of the University of Basel. **Author contributions:** L.T.J. and R.L. conceptualized the study. R.M., E.A., G.C., T.S., L.T.J., and R.L. developed the methodology. E.A. wrote the code. E.A. and R.L. ran computational analyses. R.M. and G.C. performed wet laboratory experiments. R.M., E.A., and R.L. generated the figures. E.A., T.S., and L.T.J. acquired funding. L.T.J. and R.L. wrote the original draft of the manuscript. R.M., E.A., G.C., T.S., L.T.J., and R.L. reviewed and edited the manuscript. R.M., L.T.J., and R.L. administered the project. R.M., T.S., L.T.J., and R.L. supervised the study. **Competing interests:** R.M., T.S., L.T.J., and R.L. are cofounders and hold equity of Cimeio Therapeutics AG (Cimeio) and are inventors on granted patents and patent applications related to immune cell engineering. L.T.J. is a Cimeio board member, has a sponsored research agreement with Cimeio, has received speaker fees from Novartis, and is a paid consultant for Kyowa Kirin. R.L. is a paid consultant for Memo Therapeutics. All other authors declare that they have no competing interests. **Data and materials availability:** All data associated with this study are present in the paper or the Supplementary Materials. Plasmids containing the variants will be made available through Addgene or will be made available upon reasonable request. Code for the variant annotation pipeline (version 1.3.0) is openly available on GitHub (*91*).

Submitted 2 May 2025
Accepted 20 November 2025
Published 17 December 2025
10.1126/scitranslmed.ady4877